Investigation of Doppler Effects on the Detection of Polyphase Coded Radar Waveforms

Geoffrey G. Bowman

INVESTIGATION OF DOPPLER EFFECTS ON THE DETECTION OF POLYPHASE CODED RADAR WAVEFORMS

THESIS

Geoffrey G. Bowman, Second Lieutenant, USAF

AFIT/GCE/ENG/03-01

DEPARTMENT OF THE AIR FORCE
AIR UNIVERSITY

AIR FORCE INSTITUTE OF TECHNOLOGY

APPROVED FOR PUBLIC RELEASE, DISTRIBUTION UNLIMITED

The views expressed in this thesis are those of the author and do not reflect the official policy or position of the united States Air Force, Department of Defense or United States Government.

INVESTIGATION OF DOPPLER EFFECTS ON THE

DETECTION OF POLYPHASE CODED RADAR

WAVEFORMS

THESIS

Presented to the faculty of the Graduate School of Engineering & Management

of the Air Force Institute of Technology

Air University

In Partial Fulfillment of the

Requirements for the Degree of

Master of Science (Computer Engineering)

Geoffrey G. Bowman, B. S.

Second Lieutenant, USAF

February 2003
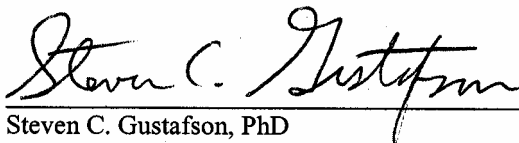
INVESTIGATION OF DOPPLER EFFECTS ON THE

DETECTION OF POLYPHASE CODED RADAR
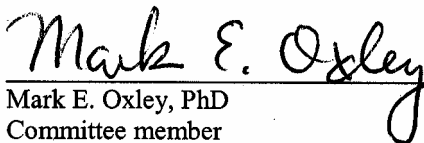
WAVEFORMS

THESIS

Geoffrey G. Bowman, B. S.
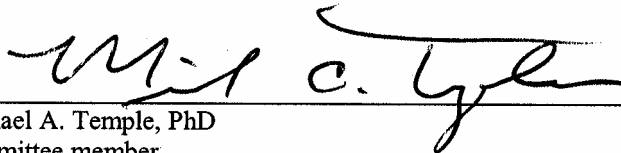Second Lieutenant, USAF

Approved:

Steven C. Gustafson, PhD
Chairman

7 Mar 03
Date

Mark E. Oxley, PhD
Committee member

7 Mar 03
Date

Michael A. Temple, PhD
Committee member

7 Nov 03
Date

3

Acknowledgements

First, I would like to thank my advisor, Dr. Gustafson. He gave me great latitude in my research and let me go wherever I wanted, but always ensured I didn't stray too far off path. I would also like to thank my committee members, Dr. Temple and Dr. Oxley, for all of their mentorship and advice on completing this document, and for approving it after it was completed!

Next, thanks should be given to all my friends at AFIT who in their various ways kept me on track and able to accomplish this task. In particular, I would like to thank Capt. John Kurian and Lt. Courtney Canadeo for all of their help with MATLAB coding issues. Without them I would have had to use the built in help libraries; an unappealing thought to say the least.

Finally, I want to thank all of my professors both here and in my education up to here. Without these teachers I could have accomplished nothing. I may have whined and complained the whole way through the process, but if I've made it this far they must have done their jobs well.

<div align="right">Geoffrey G. Bowman</div>

Table of Contents

List of Figures

8

Abstract

Special operations missions often depend on discrete insertion of highly trained soldiers into dangerous territory. To reduce the risk involved in this type of engagement, Low Probability of Detection radar waveforms have been designed specifically to defeat enemy passive radar detectors. These waveforms have been shown to perform well when the Doppler shift is minimal, but their performance degrades dramatically with increased frequency shifts due to Doppler effects.

This research compares one known Low Probability of Detection waveform, based on Welti coding, with a radar waveform known to provide Doppler constancy, namely, one based on Frank coding. These waveforms are tested using a non-cooperative square-law passive detector as well as a cooperative matched filter detector for various Doppler shift values. Research conclusions address the question of whether or not the Frank coded waveforms provide better detection capability than Welti coded waveforms at high levels of Doppler shift.

Conclusions from this research indicate that there is no advantage to using Frank coded waveforms over Welti coded waveforms. All waveforms behaved the same at increasing Doppler shift levels for each of the detectors.

INVESTIGATION OF DOPPLER EFFECTS ON THE DETECTION OF POLYPHASE CODED RADAR WAVEFORMS

Chapter 1 Introduction

This thesis compares two radar modulation schemes against two radar detectors at different Doppler shift levels. Chapter 1 presents the thesis problem statement, as well as thesis goals and the organization of this document.

1.1 *Problem Statement*

Recent studies have evaluated coded radar waveforms based on their performance against different inexpensive passive non-cooperative detectors [1]. However, these experiments have been limited to radars working only in terrain following (TF) modes. In preliminary tests, these modulation schemes experience a drop-off in detection capabilities with increased Doppler shifts. Doppler shifts are not a concern in TF applications because the difference in velocity between the ground and the radar emitter is known and is often relatively small. However, radar systems designed to detect enemy aircraft experience unknown Doppler shift that may be very large.

A study of waveforms resistant to Doppler shift is needed. This study tests the Frank polyphase coded waveform, known for its resistance to Doppler shift [3], against the Welti coded waveform, known for its performance in TF applications [1]. The two code types are tested for their detectability against two different radar detectors, the non-cooperative square-law, an inexpensive passive detector, and the cooperative matched filter. These waveforms are also tested at different levels of Doppler shifts.

1.2   Thesis Goal

The goal of this thesis is to determine the capabilities of the Frank versus the Welti coded waveforms. The evaluation parameters indicate detection capability by the non-cooperative square-law detector as well as the detection capabilities of the various waveforms with the cooperative matched filter detector. The different waveforms are tested according to different Doppler shift levels as well to simulate their performance in Air-to-Air radar applications.

1.3   Thesis Organization

This document is organized as follows. Chapter 2 defines the problem and provides relevant background information needed to understand the experiments and conclusions. Chapter 3 discuses the methodology used in designing the experiments. Chapter 4

presents results of the experiments described in Chapter 3. Chapter 5 gives the

conclusions drawn from the experimental results as well as suggested follow-on research.

Chapter 2   Background

2.1   Radar Waveforms

The use of electromagnetic waves for the express purpose of detecting targets dates back to the beginning of World War II [4]. Since then, many technological and theoretical developments have served to improve radar detection range and resolution. Radar waveforms have evolved along with other radar technologies. The original radar waveforms, rectangular gated sinusoids, have many good properties and are still used today in numerous applications. However, radar systems using these waveforms are easily detected by unintended receivers. This feature is undesirable for special operations and stealthy airframes whose survivability greatly depends on completing missions undetected. Thus, radar pulses are now usually coded.

Radar waveform coding may degrade detection range and range resolution while lowering an opponent's detection ability. Coded waveforms that maintain reasonable detection range and range resolution capabilities while being more difficult to detect are called Low Probability of Detection (LPD) waveforms [1]. LPD waveforms allow radars to actively scan in hostile areas with reduced risk of enemy detection.

2.1.1 Terrain Following and Air-to-Air Radars

Two important radar applications are Terrain Following and Air-to-Air (AA) surveillance. TF radars provide pilots an extended and accurate view of their altitude and the upcoming area. This type of scanning is used in terrain masking missions and experiences only minor Doppler effects, which are easily compensated for using knowledge of the aircraft speed. Several coded waveforms have been developed that possess good LPD properties and are useful for TF radars [1].

In contrast, AA scanning radars typically encounter a wide range of Doppler, which decreases the radar range and resolution properties. Certain coded waveforms are more resistant to Doppler than others. Searching for Doppler resistant AA waveforms and determining their probability of detection is the focus of this research.

2.1.2 Waveform Construction

A radar waveform consists of several parts. First there is the carrier, which is a sinusoid wave set at a certain frequency and amplitude according to the radar application. Typical modern radar frequencies range from tens of MHz to hundreds of GHz [2]. Equation 2.1 shows a general carrier wave equation where the values A and f are the amplitude and frequency, respectively, and where t is the independent variable time.

$$w_c = A \cdot \sin(2\pi \cdot f \cdot t) \qquad \textbf{(2.1)}$$

The second part of a radar waveform is the modulation, for which there are various types in use today. Amplitude modulation (AM) and frequency modulation (FM) are two modulation techniques commonly known for their use in radio. A third type of modulation, phase modulation (PM), is used in this research. The properties of PM are described in the following section. Modulation is applied to the carrier wave to transmit information or change the carrier's properties.

2.1.2.1   Phase Modulation

Modulation may be applied to the carrier in various ways. In the case of PM, a set of phase changes, known as the phase modulation code, is applied to the carrier during specified intervals. Adding phase change value Φ_i to the sinusoid, as seen in Equation 2.2, varies the phase of the wave.

$$w = A \cdot \sin(2\pi \cdot f_c \cdot t + \Phi_i) \qquad \textbf{(2.2)}$$

Each phase change value is maintained for a certain number of carrier periods before the phase is shifted again. The length of a single phase shift is known as the chip length (T_c). A PM waveform can be considered a piecewise sinusoidal function with each chip being a separate piece of the complete wave.

Consider the following example. Equation 2.3 has a PM code with two phase values, π and $\pi/2$. Chip length T_c equals one period. Figure 2.1 shows the PM waveform.

$$w = \begin{cases} \sin(2\pi \cdot t) \, , & 0 \le t < 200 \\ \sin(2\pi \cdot t + \pi) \, , & 200 \le t < 300 \\ \sin(2\pi \cdot t + \dfrac{\pi}{2}) \, , & 300 \le t < 400 \\ \sin(2\pi \cdot t) \, , & 400 \le t < 600 \end{cases} \qquad \textbf{(2.3)}$$
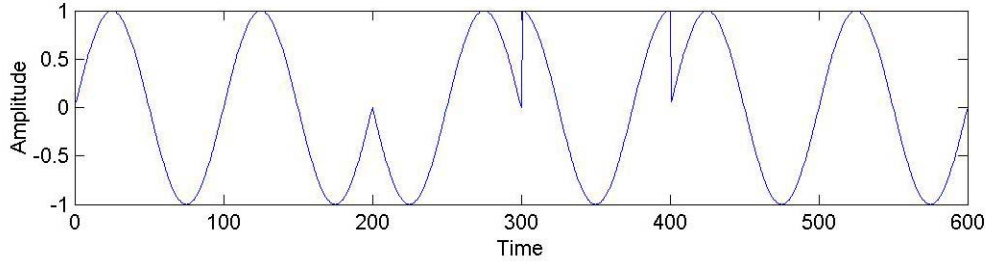
Figure 2.1: PM waveform described in Equation 2.3.

Note the sudden jumps in the sinusoid at t = 200, 300, and 400. These jumps correspond to phase discontinuities resulting from the phase modulation scheme. The next section discusses a particular set of phase modulated waveforms based on Frank coding.

2.1.2.2   Frank Codes

Frank codes are the particular type of PM code evaluated in this research. These codes are considered because of their resistance to the effects of Doppler shifts [3]. The Frank code phase shifts are determined from an N-by-N matrix. Code length N, and a particular matrix row each define a separate code set in this research. The nomenclature for Frank codes used here is as follows: Frank (N, row). For example, Frank (13,7) indicates a code corresponding to the seventh row of the length 13 Frank code matrix.

16

To create a Frank code, first choose a code length N, a positive integer. The values of row 1 of the matrix are all zero. The values in the second row are [0*360˚/N] mod 360˚, [1*360˚/N] mod 360˚, [2*360˚/N] mod 360˚, and so on up to [N*360˚/N] mod 360˚. The values in the third row are equal to [0*360˚/N] mod 360˚, [2*360˚/N] mod 360˚, [4*360˚/N] mod 360˚, and so on up to [2N*360˚/N] mod 360˚. This process is repeated up through row N. The following example goes step-by-step through the construction of a Frank code of length 5.

Example 2.1: Creation of a length 5 Frank code matrix

```
Code length: N = 5

Phase shift: 360 / 5 = 72

Row 1: [0, 0, 0, 0, 0]

Row 2: [mod(0*72,360), mod(1*72,360), mod(2*72,360), mod(3*72,360),
mod(4*72,360)]
      = [0, 72, 144, 216, 288]

Row 3: [mod(0*72,360), mod(2*72,360), mod(4*72,360), mod(6*72,360),
mod(8*72,360)]
      = [0, 144, 288, 72, 216]

Row 4: [mod(0*72,360), mod(3*72,360), mod(6*72,360), mod(9*72,360),
mod(12*72,360)]
      = [0, 216, 72, 288, 144]

Row 5: [mod(0*72,360), mod(4*72,360), mod(8*72,360), mod(12*72,360),
mod(16*72,360)]
      = [0, 288, 216, 144, 72]

Final Frank 5 matrix:   [0,   0,   0,   0,   0]
                        [0,  72, 144, 216, 288]
                        [0, 144, 288,  72, 216]
                        [0, 216,  72, 288, 144]
                        [0, 288, 216, 144,  72]
```

2.1.2.3   Welti Codes

Welti codes are another type of phase modulation scheme. These codes are known to have good performance in TF modes, but experience correlation magnitude drop off with increased amounts of Doppler shift [1].

All Welti codes are created from the same two starting vectors, (1,1) and (1,0). These vectors are divided into halves, w x y and z, and re-combined in four ways. Example 2.2 goes through the method used to create four $N = 4$ Welti codes.

Example 2.2: Creation of length 4 Welti codes

```
Initial code vector 0: D₀¹ = (1,1)
Initial code vector 1: D₁¹ = (1,0)
D₀¹(1) = w = 1
D₀¹(2) = x = 1
D₁¹(1) = y = 1
D₁¹(2) = z = 0
D₀² = (w,x,w,x⁻¹) = (1,1,1,0)
D₁² = (w,x,w⁻¹,x) = (1,1,0,1)
D₂² = (y,z,y,z⁻¹) = (1,0,1,1)
D₃² = (y,z,y⁻¹,z) = (1,0,0,0)
```

These four new codes can be used to create eight $N = 8$ codes in the same manner. A Welti code set consists of 2^N codes of length 2^N created as shown in Example 2.2 [1].

The next section describes the Doppler effect and why it is a problem in radar detection.

2.2 Doppler Effect

The Doppler effect important to this research is the same as is encountered in day-to-day life. For example, whenever an emergency vehicle rushes past a slower moving vehicle or stationary person, the Doppler effect causes the change in pitch. In the radar world, the interest in Doppler lies in how it changes the radar waveform as it reflects from moving targets. Objects with large differential velocities (for instance, two supersonic fighter jets) experience detection range degradation due to Doppler. The drop off in performance can be compensated for using additional hardware, but the need for more hardware further complicates the radar system design.

The Doppler frequency shift equation is shown in Equation 2.4 [4]. Doppler shift f_d is the overall change in frequency due to the relative velocity between the source and the destination v_r. Wavelength λ, equals the speed of light c divided by transmitted frequency fc.

$$f_d = \frac{2v_r}{\lambda} = \frac{2f_c v_r}{c} Hz \qquad \textbf{(2.4)}$$

In Example 2.3, Equation 2.4 is used to determine the Doppler Shift experienced shift seen when there is a differential velocity of Mach 1, 332 m/sec in air at 0° C.

Example 2.3: Using the Doppler frequency shift equation

```
Speed of sound in air at 0 C: v_r = 332 m/sec

Transmitted frequency: f_t = 1 GHz = 1 * 10^9 Hz

Speed of light: c = 3 * 10^8 m/sec

f_d = (2 * (1 * 10^9 Hz)*( 332 m/sec)) / ( 3 * 10^8 m/sec) = ⌐2210 Hz¬
```

Thus, the final carrier frequency is 1,000,002,210 Hz. The next section describes an analysis tool for the effects of Doppler shifts, the ambiguity diagram.

2.3 Ambiguity Diagrams

The ambiguity diagram is a waveform analysis tool. It is a three-dimensional plot that represents the matched filter output at different Doppler shift levels and range delays. Ambiguity diagram data points come from correlating the returning waveform with a filter set as the outgoing waveform. Section 2.3.1 describes the correlation process.

2.3.1 Correlation

Correlation is a process whereby vectors are multiplied and summed in an iterative fashion. Equation 2.5 describes the correlation function. When y_1 equals y_2, function $\Phi[t]$ is known as the auto-correlation of y_1 and when they are unequal, the function is known as the cross-correlation of y_1 and y_2.

$$\Phi[t] = \sum_{-\infty}^{\infty} y_1[\lambda] y_2[\lambda - t]$$
$$t = \{...-2,-1,0,1,2...\}$$

<div align="right">(2.5)</div>

Example 2.4 shows how a square wave of length five goes through the auto-correlation process.

Example 2.4: Auto-correlation of a length five square wave

```
Square wave: y₁ = y₂ = [. . . 0, 0, 0, 1, 1, 1, 1, 1, 0, 0, 0 . . .]

t = 1
y₁                          [. . . 0, 1, 1, 1, 1, 1, 0 . . .]
y₂                   [. . . 0, 1, 1, 1, 1, 1, 0 . . .]
```

$\Phi[1] = 1*1 = 1$

```
t = 2
y₁                          [. . . 0, 1, 1, 1, 1, 1, 0 . . .]
y₂                 [. . . 0, 1, 1, 1, 1, 1, 0 . . .]
```

$\Phi[2] = 1*1 + 1*1 = 2$

```
t = 3
y₁                          [. . . 0, 1, 1, 1, 1, 1, 0 . . .]
y₂               [. . . 0, 1, 1, 1, 1, 1, 0 . . .]
```

$\Phi[3] = 1*1 + 1*1 + 1*1 = 3$

```
t = 4
y₁                          [. . . 0, 1, 1, 1, 1, 1, 0 . . .]
y₂             [. . . 0, 1, 1, 1, 1, 1, 0 . . .]
```

$\Phi[4] = 1*1 + 1*1 + 1*1 + 1*1 = 4$

```
t = 5
y₁                          [. . . 0, 1, 1, 1, 1, 1, 0 . . .]
y₂                          [. . . 0, 1, 1, 1, 1, 1, 0 . . .]
```

$\Phi[5] = 1*1 + 1*1 + 1*1 + 1*1 + 1*1 = 5$

```
t = 6
y₁                          [. . . 0, 1, 1, 1, 1, 1, 0 . . .]
y₂                            [. . . 0, 1, 1, 1, 1, 1, 0 . . .]
```

$\Phi[6] = 1*1 + 1*1 + 1*1 + 1*1 = 4$

```
t = 7
```

Y₁   [. . . 0, 1, 1, 1, 1, 1, 0 . . .]
Y₂   [. . . 0, 1, 1, 1, 1, 1, 0 . . .]

Φ[7] = 1*1 + 1*1 + 1*1 = 3

t = 8
Y₁   [. . . 0, 1, 1, 1, 1, 1, 0 . . .]
Y₂   [. . . 0, 1, 1, 1, 1, 1, 0 . . .]

Φ[8] = 1*1 + 1*1 = 1

t = 9
Y₁   [. . . 0, 1, 1, 1, 1, 1, 0 . . .]
Y₂   [. . . 0, 1, 1, 1, 1, 1, 0 . . .]

Φ[9] = 1*1 = 1

Note that $\Phi[t]$ is greatest when the two vectors are aligned, i.e., at $t = 0$ in equation 2.5. Figure 2.2 is a plot of $\Phi[t]$ for four periods of a sinusoidal carrier wave of unit amplitude and frequency. This plot is equivalent to the zero Doppler shift line of the ambiguity diagram.
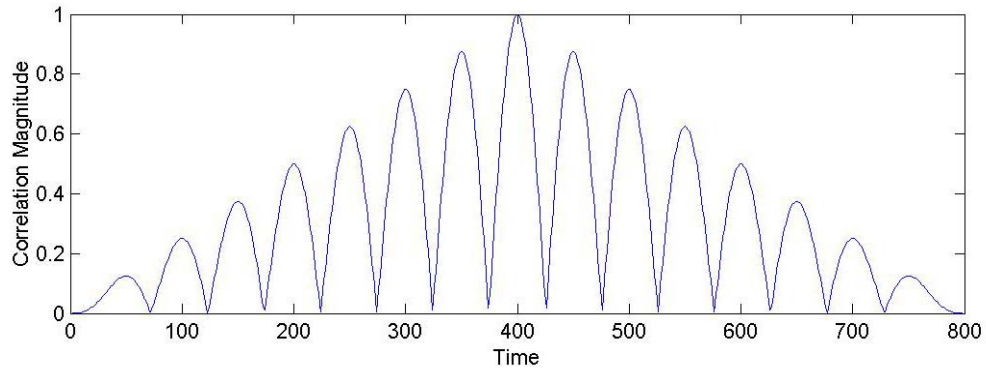
Figure 2.2: Auto-correlation of a sine wave

The correlation magnitude is normalized such that the peak value equals one. The absolute value of the correlation magnitudes is used throughout this research. The correlation mainlobe in Figure 2.2 is the function response from approximately 375 to 425, the bump that includes the peak value. The other bumps are called sidelobes.

2.3.2 Parts of an Ambiguity Diagram

Figure 2.3 is an ambiguity diagram of Frank (13, 13). The range delay axis is normalized to range from −1 to 1 such that the peak always occurs at 0. The correlation magnitude axis is normalized and expressed in dB.
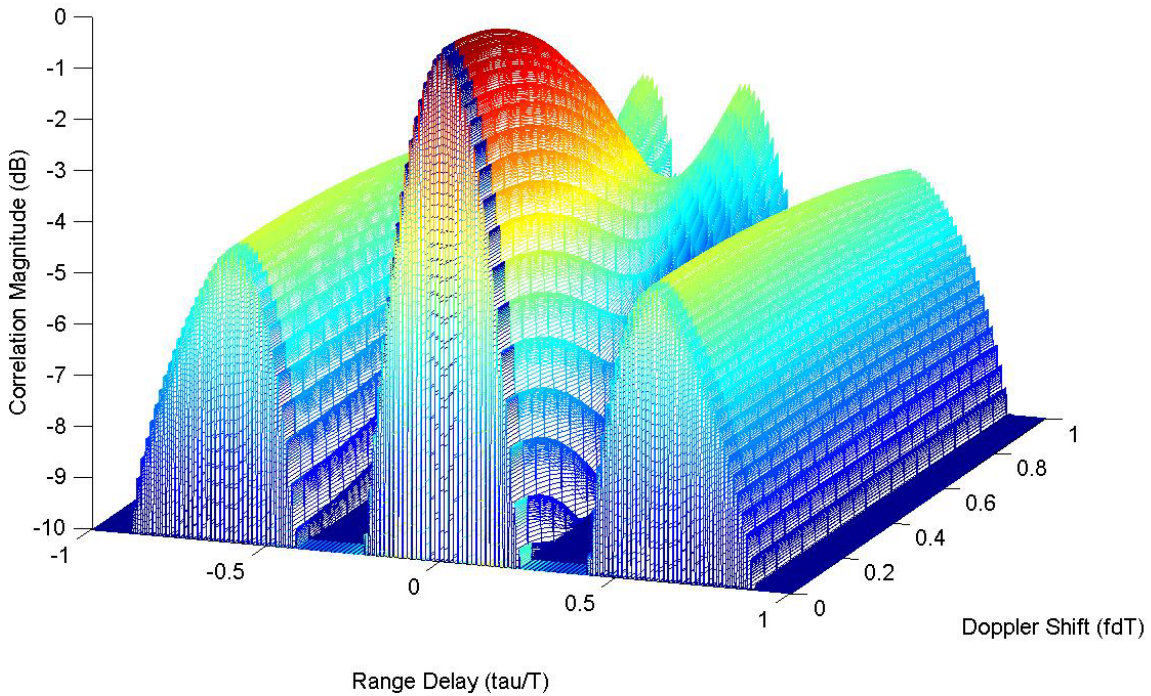
Figure 2.3: Ambiguity diagram of Frank (13, 13)

Note the drop-off of correlation magnitude at higher levels of Doppler shift. The resistance of Frank codes to this degradation is the reason that they are considered here.

2.4 Detectors

Two different detectors are used in this research. The first, the matched filter detector mentioned earlier, consists of sophisticated hardware. The second, the square-law

detector, is a simple and inexpensive device used to detect radar waveform presence. The matched filter detector is a form of cooperative detection because the receiver (detector) knows what waveform it is looking for. The square-law detector is non-cooperative because it uses no knowledge of the received waveform structure to determine if radar is actively scanning in the area.

2.4.1 Matched Filter Detector

The cooperative matched filter is designed the give a greater probability of detection for lower signal-to-noise ratios. It accomplishes this task by correlating the incoming signal with a perfect copy of the outgoing signal. When the incoming signal is only noise, the correlation values are minimal. However, when the incoming signal is the waveform plus noise, the correlation values are greatly increased. The design of a matched filter detector requires knowledge of the waveform frequency and modulation. Without these parameters, the capabilities of the detector are significantly degraded. Figure 2.4 is a diagram of the matched filter detector.
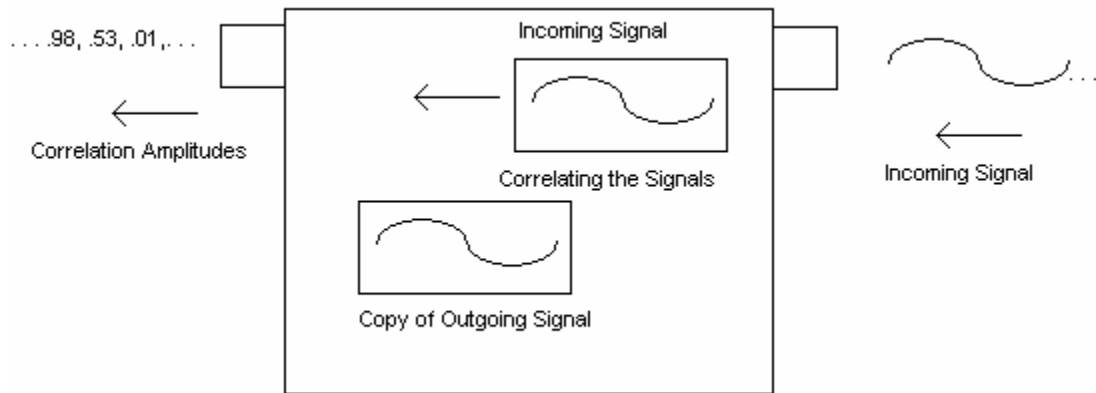
Figure 2.4: Diagram of the matched filter detector

The incoming signal can be background radiation modeled as random independent Gaussian white noise, or noise plus the outgoing signal. The incoming signal is then correlated with a matched copy of the outgoing signal. If the incoming signal and the copy of the outgoing signal match up, then the correlation magnitudes will be high and detection can be declared. If the input signal is only background noise, the correlation will yield small values and detection will not be declared. The value which a correlation magnitude must exceed in order to declare detection is called the threshold. A threshold value is chosen for a particular probability of false alarm (P_{fa}). For example, a threshold level chosen for a P_{fa} of .001 indicates that only 1 in a thousand noise realizations, when correlated with a copy of the outgoing waveform, yield a correlation magnitude greater than the threshold. Figure 2.5 shows a correlation plot of one noise realization with the copy of the outgoing signal (the lower non-constant values), the correlation of an addition of the outgoing signal and the noise realization (the upper non-constant values), and the threshold value (the upper constant value). In this case, the matched filter detector does

not declare detection because nowhere does the correlation magnitude exceed the threshold value.
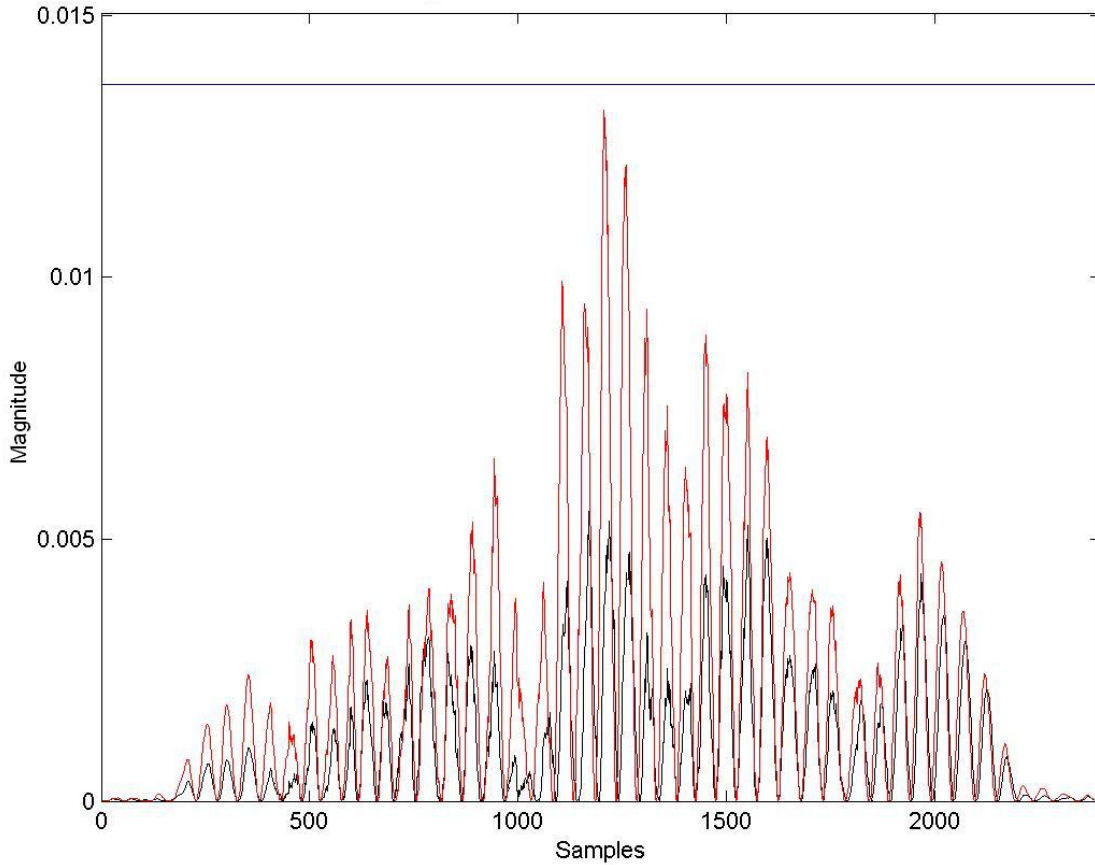
Figure 2.5: Example of matched filter detection process

Collections of these detections at different signal-to-noise ratios are known as Receiver Operating Characteristic (ROC) curves. ROC curves show the probability of detection at various signal-to-noise ratios. Figure 2.6 is a ROC curve for a matched filter detector where the signal used is a Frank 13,13 coded waveform. Each data point is based on the detection of the signal plus one hundred independent realizations of Gaussian noise. The P_{fa} in this figure is 0.01.
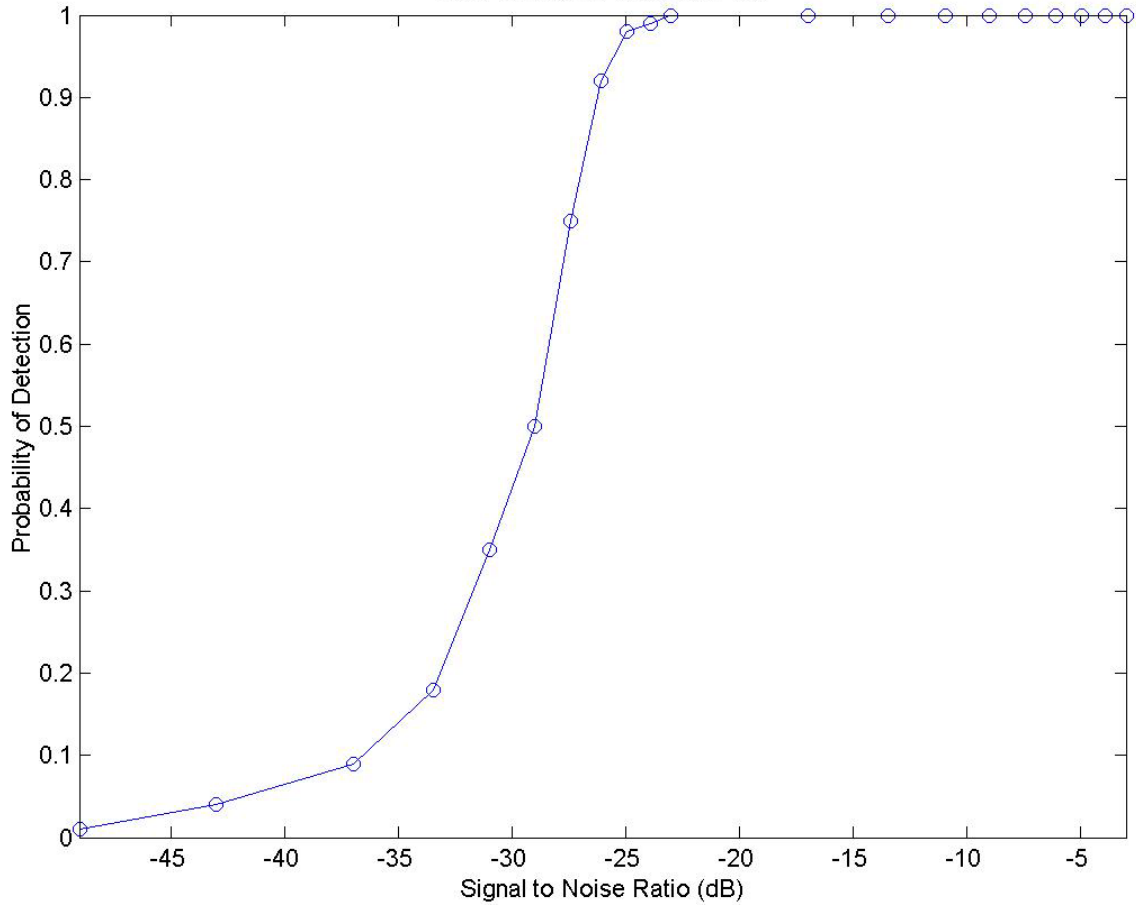
Figure 2.6: ROC curve for matched filter detection of a Frank (13,13) coded waveform
with Pfa = .01

2.4.2 Square-law Detector

The non-cooperative square-law detector is an inexpensive way for an unsophisticated
enemy to detect the presence of active radar scanning in an area. It is known as a passive
detector because no signal is sent out for the detection process. Also, designers of the
square-law detector do not need to know anything about the incoming signal. The
detector collects a certain number of samples of the incoming signal during a detection

27

interval. These samples are then squared and summed to give their average power in that interval. If this average power is greater than some pre-determined threshold value, detection is declared. Figure 2.7 is one example of the detection process used in a square-law detector. The dotted line is the incoming signal. The constant line is the threshold level. The thick line is the average power per interval. In this example, the detection interval is set to 100 samples. This signal is a PM waveform with two phases, $\pi/2$ and $2\pi/7$. The period of the waveform is equal to 100 samples. The threshold value is set according to a P_{fa} of 0.001. For Figure 2.7, detection is declared because the average power of at least one detection interval is greater than the threshold.
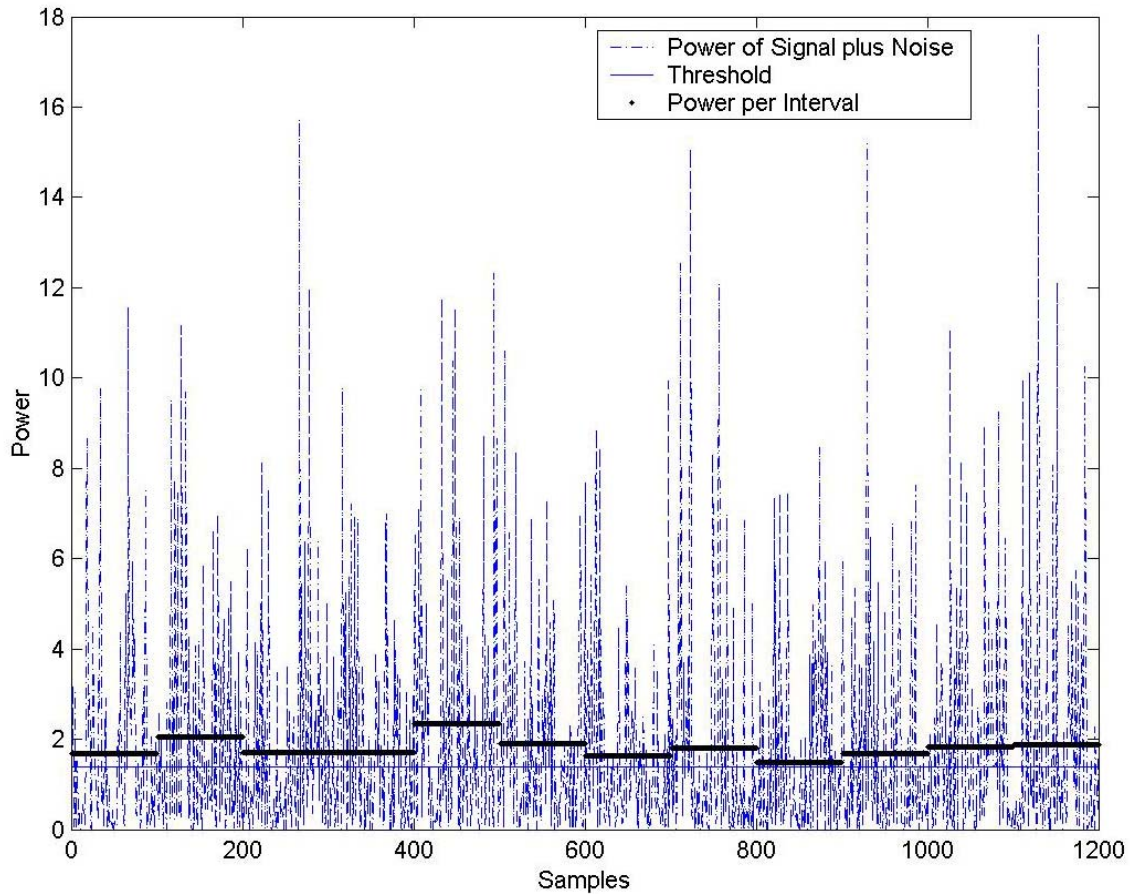
Figure 2.7: Example of square-law detection process

The detection interval values in this example do not depend on the input waveform. These values will be virtually the same for any waveform used.

Figure 2.8 is the ROC curve for a square-law detector and the waveform described above. This graph is completed in the same manner as the one found in Figure 2.6 except that it has the curves for several Pfa's. The top line is for a Pfa of 0.1, the middle 0.01, and the bottom 0.001. The top line converges to 100% detection more quickly, but has significantly more false detections.
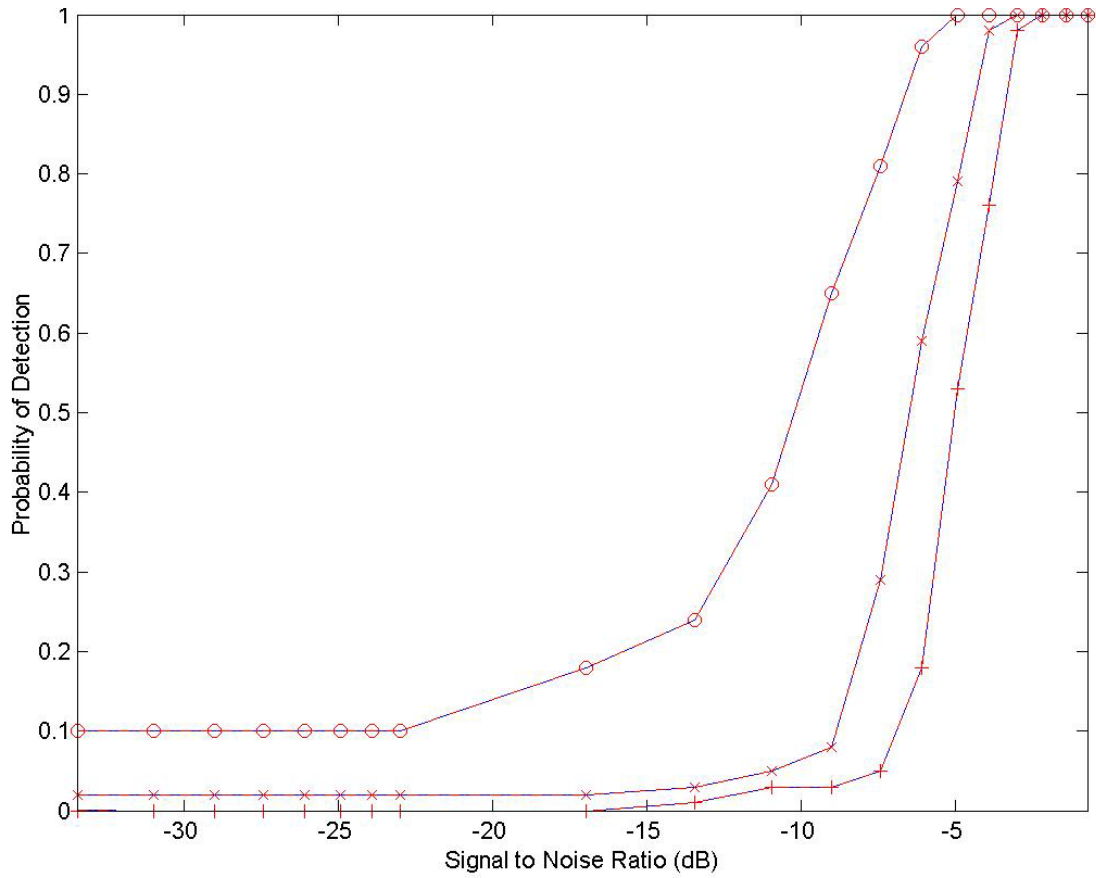
Figure 2.8: ROC curve for square-law detection of a simple PM coded waveform with
P_{fa}'s = 0.1 (o), 0.01 (x), and 0.001 (+)

Note that the signal-to-noise ratio (SNR) where 100% detection is declared is much higher in this detector than in the matched filter detector. This difference means that the matched filter detector detects a waveform much better than the square-law detector. However, enemies may not always know the frequency and encoding of their opponent's radar waveforms and therefore may not be able to use matched filter detectors.

Chapter 3 describes the methodology used in designing experiments for this research.

Chapter 3 Methodology

3.1 Problem Definition, Goals, and Approach

Stealth aircraft have the ability to fly undetected through an opponent's airspace when the opponent employs active radar scanning. However, when flying stealthy these aircraft have limited ability to view the outside world. As soon as the aircraft activates any radar device, it is susceptible to enemy radar detectors and therefore loses its stealth properties.

US military special operations often involve the insertion of small units of highly trained soldiers with very specific objectives. These units have limited firepower and staying ability. The success of their missions is based on their ability to get into and out of the mission area undetected. Using terrain-masking techniques with LPD TF radars is one way to escape detection. However, there are no current methods that allow for the long-range detection of enemy aircraft without sending out Air-to-Air (AA) radar waveforms and thereby risking detection by enemy passive detectors.

The purpose of this research is to analyze radar waveforms that are resistant to the effects of the large Doppler shifts seen in air-to-air applications and to assess their detectability to certain non-cooperative radar detectors. The waveforms most resistant to Doppler shifts are further analyzed. These waveforms are compared to capable TF waveforms to determine the improvement in resisting the effects of Doppler shifts. Waveforms are

evaluated by finding their receiver operating characteristics for different types of radar signal detectors and different modulations.

This thesis analyzes the detection properties of an AA radar waveform. There are numerous codes that have been developed with either good detection or AA properties, but none with both. Testing every type of code is not possible, therefore Frank ploy-phase codes are the waveforms tested because of their resistance to Doppler shifts [3]. These are also the codes chosen by the sponsor for testing. The best Frank coded waveforms are compared to Welti codes, which are known to have good detection capabilities but which are susceptible to degradation due to Doppler shifts [1].

Different Frank coded waveforms are measured against two different detectors: square-law and matched filter. Finally, a Welti coded waveform is measured against the same detectors for purposes of comparison.

3.2   System Boundaries

The system under study consists of a radar pulse generator, a radar filter, and an array of radar waveform detectors. The specific component under test is the coded waveform. An abstract picture of the system is shown in Figure 3.1. Object 1 in the figure is an aircraft that uses various modulation codes to produce radar waveforms for air-to-air detection with the matched filter detector. Object 2 is a square-law detector receiver

array listening for anyone in the air space. Object 3 is the coded radar signal emitted into open space for detection.
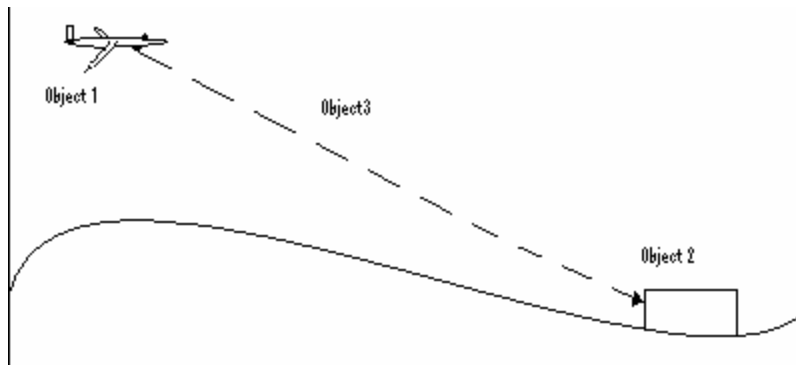
Figure 3.1: System Under Test

3.3   System Services

The system is used for the long distance detection of objects, and its single service is the production of AA waveforms. The possible outcomes of the system are a waveform that is not detected by a particular detector, and a waveform that is detected. The power levels at which the waveforms may be detected are continuous. Therefore, there is an infinite range of outcomes indicating the level (probability) of detection. This range of detection is displayed in ROC curves for the different detectors. These outcomes indicate the sensitivity level to which the square-law detector must be set for them to detect the waveform.

3.4   Performance Metrics

The waveforms produced need to maintain a high (near 1) correlation magnitude of the mainlobe over the entire Doppler shift range while maintaining low sidelobe correlation magnitudes. High mainlobe correlation magnitude constancy indicates the waveform is resistant to Doppler shifts. Figure 3.2 is an example of a Welti code ambiguity diagram. The function mainlobe begins to quickly fade at a relative Doppler shift of approximately 0.4 and falls beneath the sidelobe amplitude at a relative Doppler shift of approximately 0.6. Therefore, the Welti code is an example of a waveform that is not resistant to Doppler shifts.
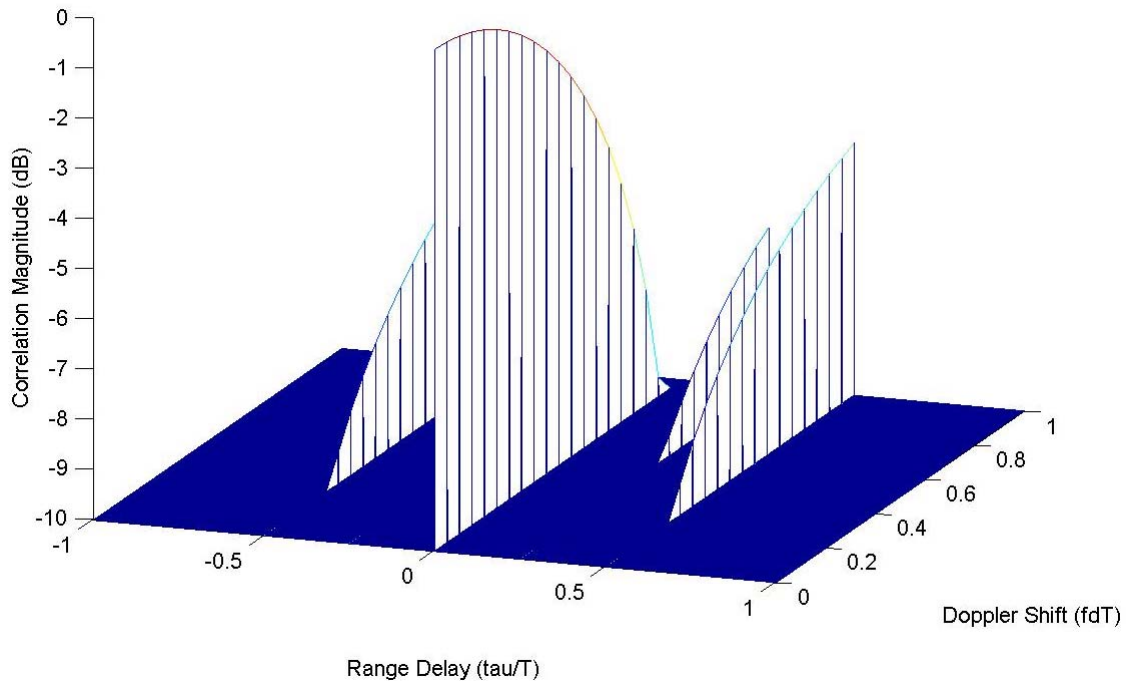
Figure 3.2: Ambiguity diagram for the Welti coded waveform

In contrast to Figure 3.2, the ambiguity diagram of a Frank coded waveform seen in Figure 3.3 shows resistance to Doppler effects. The mainlobe stays greater than the sidelobes over a majority of the Doppler shift axis.
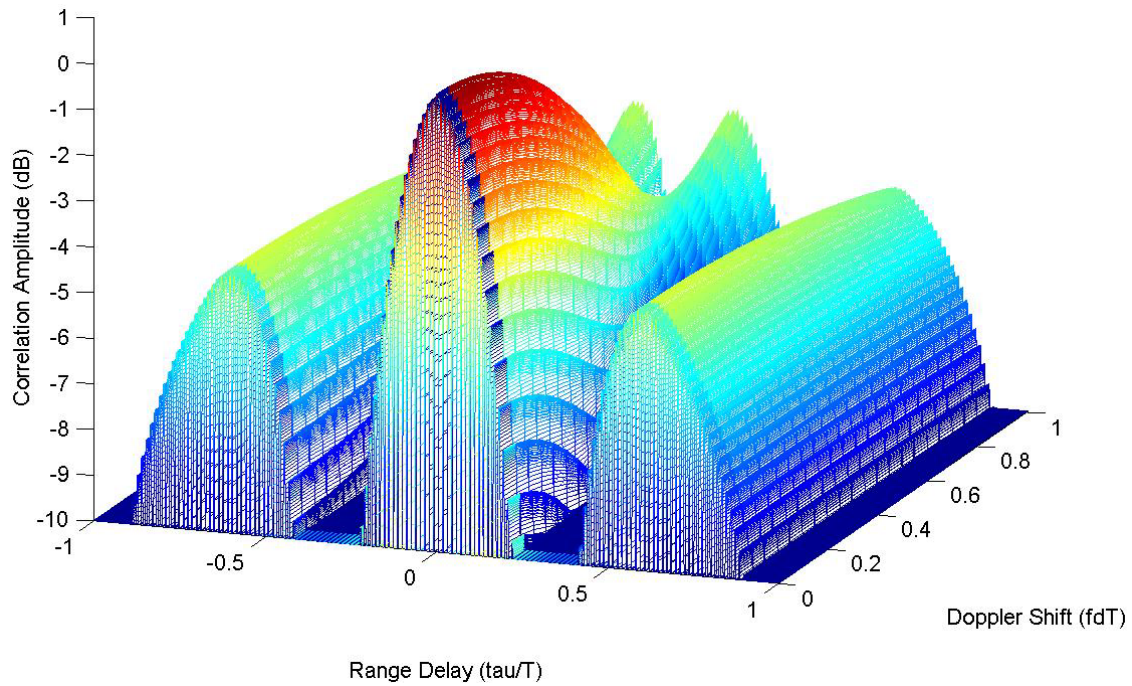
Figure 3.3: Ambiguity diagram for the Frank (13,13) coded waveform.

3.5   System

The code type is the first system parameter. Different codes types are used for different radar applications, and they have varying detection properties and levels of resistance to Doppler shifts. Changing the code type may dramatically change the system performance.

The length of code is the next system parameter. The various codes can be adjusted to whatever length is needed for the application. Previous research indicates that longer code lengths have better detection properties [1]. System performance is very sensitive to the code length used.

The type of radar detector used is a third parameter. The passive non-cooperative square-law detector has a different detection capability than the cooperative matched filter detector, and yields different ROC curve values.

The signal-to-noise ratio (SNR) is a fourth parameter. The signal power may increase from the power encountered in background radiation, while the noise power is characterized by the variance of independent Gaussian noise.

3.6   Factors

The code type is the first varied parameter of the system. The two code types selected for this thesis are Frank and Welti. Frank codes are known to have good AA properties (resistant to Doppler effects), and somewhat poorer detection properties. Welti codes were found to be the best in the FAMU-FSU College of Engineering study [1]. They have good LPD properties and are used for TF radars, but are not as resistant to Doppler shifts as Frank codes.

The next parameter varied is code length. Code lengths vary from 10 to 15 phase values for Frank coded waveforms. However, code length remains constant at 1024 phase values for the Welti coded waveform.

The final parameter varied is the SNR. Twenty different signal power levels ranging from 0 to 1.3 are combined with a constant noise variance value of 1 to create SNR values ranging from –49 dB to –0.73 dB. Equation 3.1 is used to calculate these values.

$$SNR = 10 \times \log_{10}\left(\frac{P_s}{P_n}\right) \qquad \textbf{(3.1)}$$

Variable P_s equals signal power and variable P_n equals noise power.

3.7   Evaluation Technique

This thesis is a follow-up/extension to the FAMU-FSU College of Engineering study [1], much of which was accomplished through MATLAB® simulations. The MATLAB® code used for simulations was provided for this thesis. Although extensive modifications were needed to adapt the previous code, the MATLAB® files received provided a firm foundation for evaluating the system through computer simulations.

3.8   Experimental Design

The design of the experiments for this research problem is full factorial. There are two code types, Welti and Frank. Only the best two Frank codes, according to the performance metrics discussed in Chapter 4, are evaluated. Twenty different signal-to-noise ratio values are used. Finally, twenty-one Doppler shift values are used to determine Doppler effects on the system. This yields a total of 1260 different experiments. Each experiment is executed one hundred times.

The system data is validated by ensuring independence from the random number generator seed value used. Also, discussions with MATLAB® and radar experts were used to ensure system outputs are within acceptable ranges. Finally, initial results were compared to previous research done in the 1997 FAMU-FSU College of Engineering study to verify consistency.

3.9   Analyze and Interpret Results

The data gathered is used to develop several graphs. These graphs are ROC curves and ambiguity diagrams as described in Chapter 2. The main values of concern are the SNR values at which the probability of detection is 100%. These values vary for each code and Doppler shift level. Frank codes should maintain a relatively constant ROC curve for each Doppler shift value while the ROC curves for Welti codes should degrade rapidly.

3.10 Summary

This thesis evaluates properties of two different types of coded waveforms to determine their suitability for use in air-to-air applications. Probability of detection is tested using two detectors, a matched filter and a square-law. The outcomes from the study are probability of detection values for different codes at different Doppler shift levels. These values indicate the detection capabilities of Frank coded waveforms and their resistance to Doppler shifts.

The following chapter contains results of the experiments described above.

Chapter 4 Results

This chapter presents the results of the experiments described in Chapter 3. First, the trials done with the square-law detector are presented. The next section describes how the 'best' Frank codes are chosen. Next the ambiguity diagrams for the best two Frank codes and the Welti code are compared. The final section discusses the analysis of the probabilities of detection for the various codes at different Doppler shift levels for the matched filter detector.

4.1   Square-law Detection

This first section contains the simulation details for the square-law detector. First, a description of the detection process is presented. Then, results from the square-law detector trials are complied to form a ROC curve. Finally, results from the experiments are analyzed.

4.1.1   Making a Square-law Detector ROC Curve

The square-law detector declares detection when the incoming signal average power over some interval exceeds the threshold value set for a particular P_{fa}. Figure 4.1 shows a square-law detector experiment. For this experiment, the SNR is set to -0.73 dB, the signal used is the Frank (13, 13) coded waveform, the Doppler shift amount is 0, and the

threshold is set to yield a P_{fa} of 0.01. Detection is declared in this case because the power

per interval level exceeds the threshold in at least 1 interval.
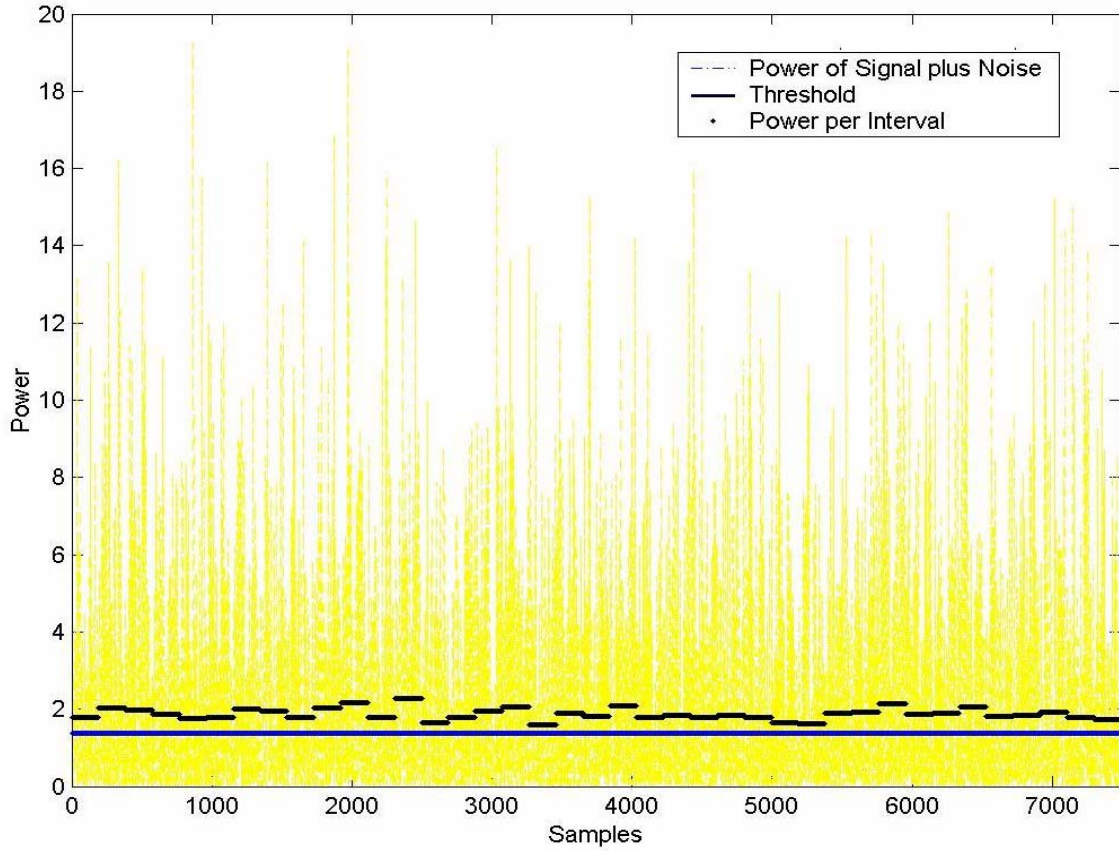
Figure 4.1: One realization of signal and noise used to find the probability of detection
for a square-law detector. Power of signal plus noise plots the squared
amplitude of each of 7488 signal samples of the Frank (13, 13) coded
waveform with independent Gaussian noise added to each sample. There are
192 samples per period, and the waveform has phase modulation consisting of
phase discontinuities between periods. The threshold is such that for 100
noise realizations of the 7488 noise samples, the average power in at least one
detection interval of length 192 samples exceeds the threshold. Thus the
probability of false alarm is 0.01. The SNR for the trial is -0.73 dB. Power
per interval plots the average signal plus noise power in each interval. Thus,
this realization counts as a detection because power per interval is above
threshold for at least one of the 39 intervals.

4.1.2 The Square-law Detector ROC Curve

The ROC curve for the square-law detector shows the probabilities of detection that are expected at varying signal-to-noise ratios. Figure 4.2 shows the ROC curve for the system described above. Each data point is a ratio of the number of detections over the number of trials run, in this case one hundred. Shifting the input signal according to some relative velocity between the sender and receiver of Mach 1 has a negligible effect on the ROC curve for a square-law detector. Note that the SNR at which 100% detection is first expected is -6 dB.
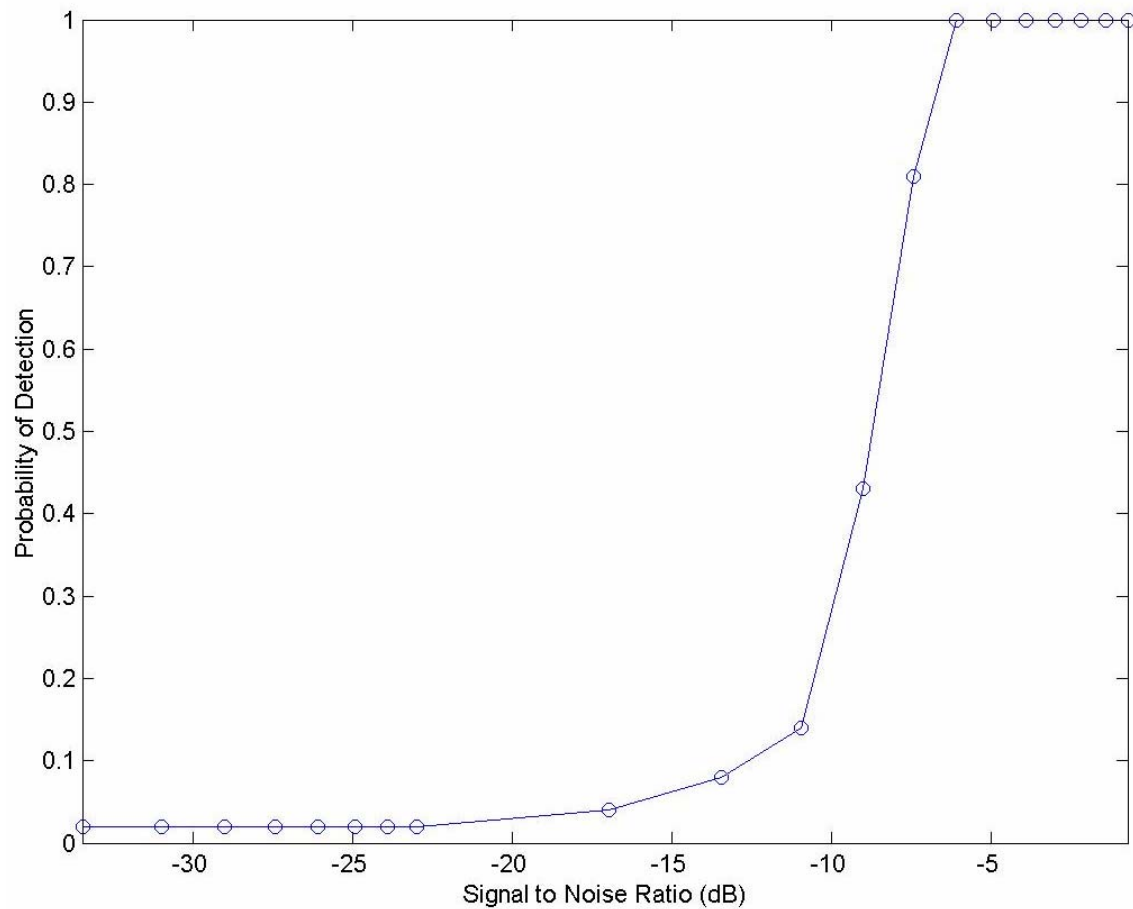
Figure 4.2: ROC curve for a square-law detector with a Frank (13, 13) coded input signal. Each point is proportional to the number of detections of a Frank (13, 13) waveform in the presence of independent Gaussian noise, where the signal to noise ratio is varied by increasing the signal amplitude. The process for declaring detection is illustrated in Figure 4.1. A Doppler shift equivalent to a difference of velocity between sender and receiver of Mach 1 had a negligible effect on these curves.

4.1.3 Results of the Square-law Detector

The square-law passive non-cooperative detector is an un-sophisticated low cost means of detecting radar signals. With the detection interval set to the same size as the received waveform period, the ROC curve will be the same for any PM waveform as well as the

carrier with equivalent signal amplitudes. Also, square-law detectors resist the effects of the Doppler shifts seen at the speed of modern aircraft. The waveforms are shifted so slightly that the change in the average power in a detection interval between an un-shifted and a shifted wave is minimal. Plots of ROC curves for the square-law detector and other modulation codes are not significantly different than the one in Figure 4.2. These additional plots are found in Appendix A.

4.2   Goodness of Codes

An infinite number of Frank codes could be analyzed. However, due to time and computing constraints, only a few of them were researched for this thesis. Because of these constraints, the Frank codes considered are of lengths ranging from 10 to 15. The first code from each of these code lengths, Frank (10, 1); Frank (11, 1); and so on, are not considered because they contain no phase shifts. This leaves a total of $9 + 10 + 11 + 12 + 13 + 14 = 69$ Frank codes to rank. This section describes how these codes are ranked and which ones are worthy of further analysis.

4.2.1 Mainlobe Constancy Metric

The first metric used to find the 'best' Frank code is the *mainlobe constancy* metric. This metric represents the standard deviation of peak values of the mainlobe of the code

ambiguity function. Mainlobe constancy is important because the more constant the mainlobe, the more resistant the waveform is to Doppler effects. This metric is a lower-better metric, meaning that the codes with the lowest values are the "best" and codes with the highest values are "worst".

4.2.2 Sidelobe to Mainlobe Ratio Metric

The second metric is the average of ratios of the peak sidelobe value to the peak mainlobe value at each Doppler shift level. This metric simply divides the greatest sidelobe value by the mainlobe value at that Doppler shift level. Each value then has the soft-max weighting function applied to it. The soft-max function weights the values such that when a ratio at a Doppler shift value is greater than 1 (indicating a sidelobe greater than mainlobe) the metric value is much larger. The soft-max weighting function is shown in Equation 4.1. In general, a lower value indicates that the mainlobe is greater than the sidelobes for a greater percentage of Doppler shift levels. A higher value means that the mainlobe falls below the sidelobe for more of the Doppler shift levels. Thus, this metric is also a lower better-metric. High mainlobes in comparison to sidelobes reduces the risk of a detection based on a sidelobe value surpassing the threshold instead of the mainlobe value.

$$m_r = n^{-1} \sum_{i=1}^{n} N(1 + e^{-k(r_i - 1)})^{-1} r_i$$

<div align="right">(4.1)</div>

$$N^{-1} = \sum_{i=1}^{n} (1 + e^{-k(r_i - 1)})^{-1}$$

The number of Doppler shifts is n, the peak sidelobe to peak mainlobe ratio at Doppler shift i is r_i, the rigidness of the sigmoid is k, and the overall metric value is m_r. The rigidness constant in this research is set to ten.

4.2.3 Combined Metric

The two metric values from the *mainlobe constancy* metric and the *sidelobe/mainlobe ratio* metric are combined into a single number. Each metric value is represented as an axis on a 2-dimensional plot. The Euclidean distance from the origin to the data values is the combined metric value. This method allows each metric to be weighted the same in importance.

4.2.4 The Best Frank Codes

Each of the 69 Frank codes with code lengths between 10 and 15 phase values were evaluated according to these metrics. The values for the 69 Frank codes and one Welti

code are shown in Figure 4.3. The best two Frank codes found according to these metrics

are Frank (13, 13) and Frank (14, 14).
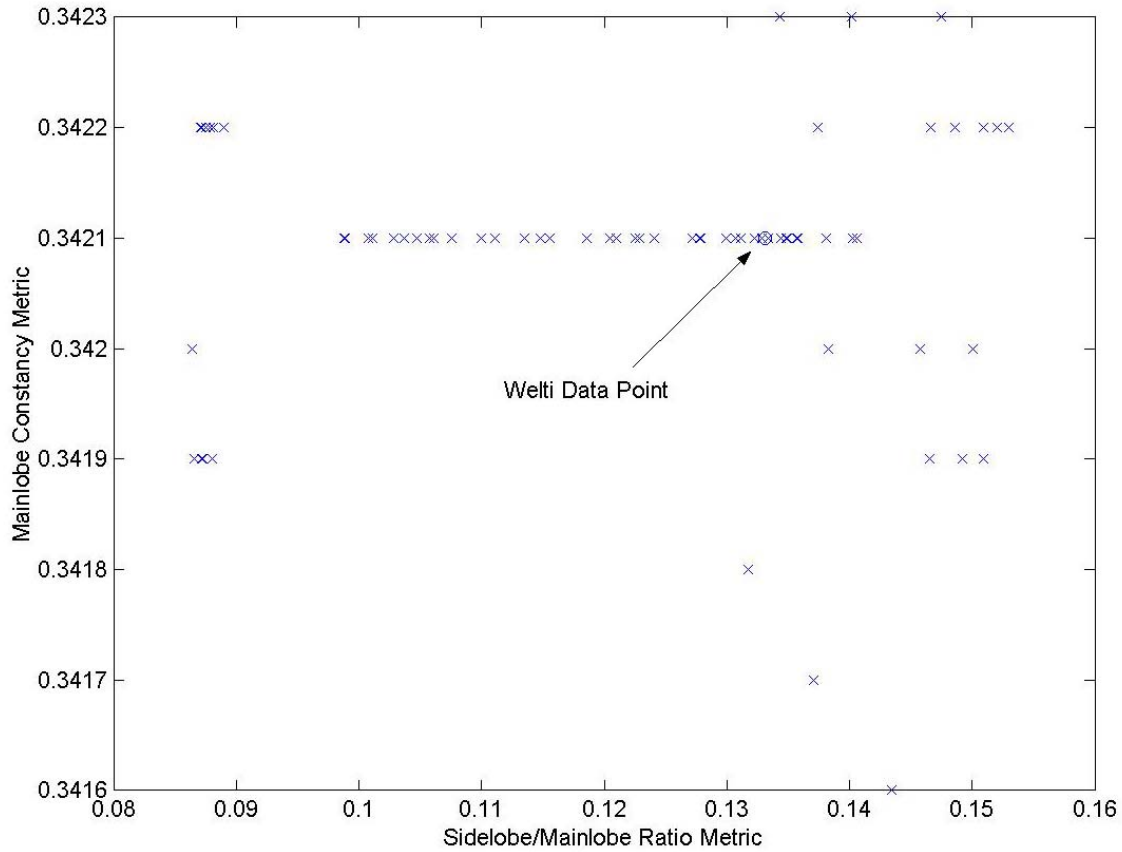
Figure 4.3: 2-Dimensional plot of metric values of various waveforms. The y-axis
contains the values of the mainlobe constancy metric described in Section
4.2.1. This metric did not vary significantly for different codes. The x-axis
contains the values for the peak sidelobe to peak mainlobe metric described in
Section 4.2.2. The Welti code's data point is pointed out in the picture. The
remaining points are the data points for the various Frank codes tested. This
chart indicates some Frank codes behave better than the Welti code according
to these metrics.

4.3   Ambiguity Diagrams

This section contains the ambiguity diagrams of the best two Frank codes, Frank (13, 13) and Frank (14, 14), as well as the Welti code.   A description of each diagram, their similarities, significant aspects, and differences precedes each diagram.

4.3.1 Frank (13, 13) Code

The best Frank code found according to metrics described in the previous section is the Frank (13, 13) code. The final combined metric value for this code is 0.3527. Figure 4.4 is the ambiguity diagram for the Frank (13, 13) coded waveform. Note how the mainlobe maintains a high mainlobe correlation magnitude across all Doppler shift values. However, the high sidelobe correlation magnitudes seen at ±0.6 on the range delay axis could cause false detections in the matched filter.
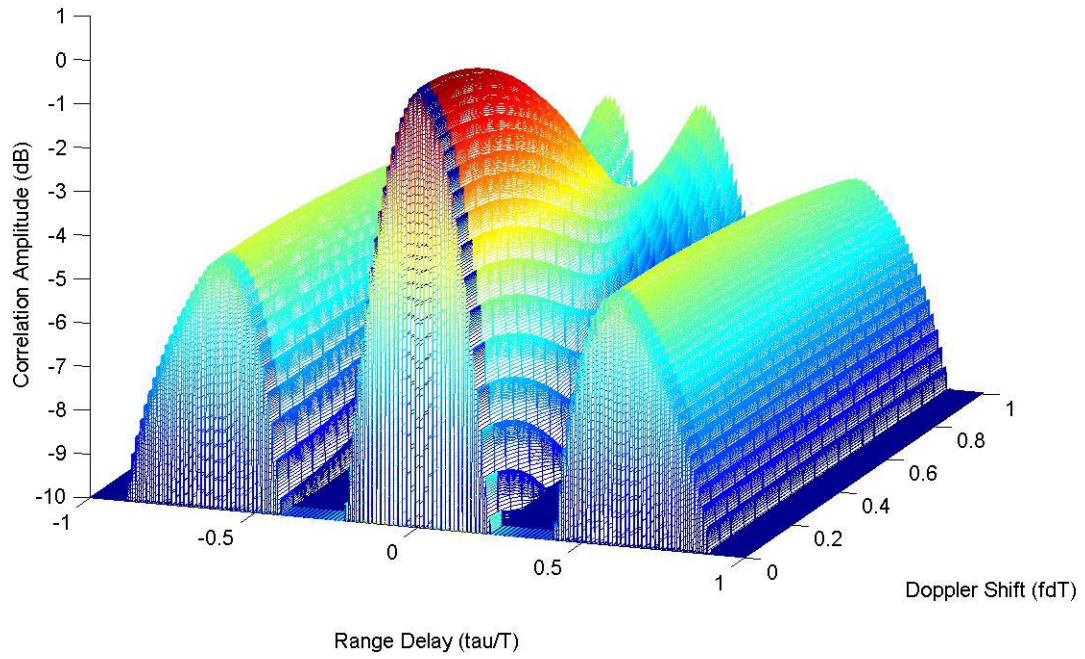
Figure 4.4: Ambiguity diagram for the Frank (13, 13) coded waveform

4.3.2 Frank (14, 14) Code

The second best Frank code according to the metrics of Section 4.2 is the Frank (14, 14) code. The final combined metric value for this code is also 0.3527. Figure 4.5 shows the ambiguity diagram for the Frank (14, 14) coded waveform. This figure is very similar to Figure 4.4. All the comments for the Frank (13, 13) ambiguity diagram also apply to the Frank (14, 14) ambiguity diagram.
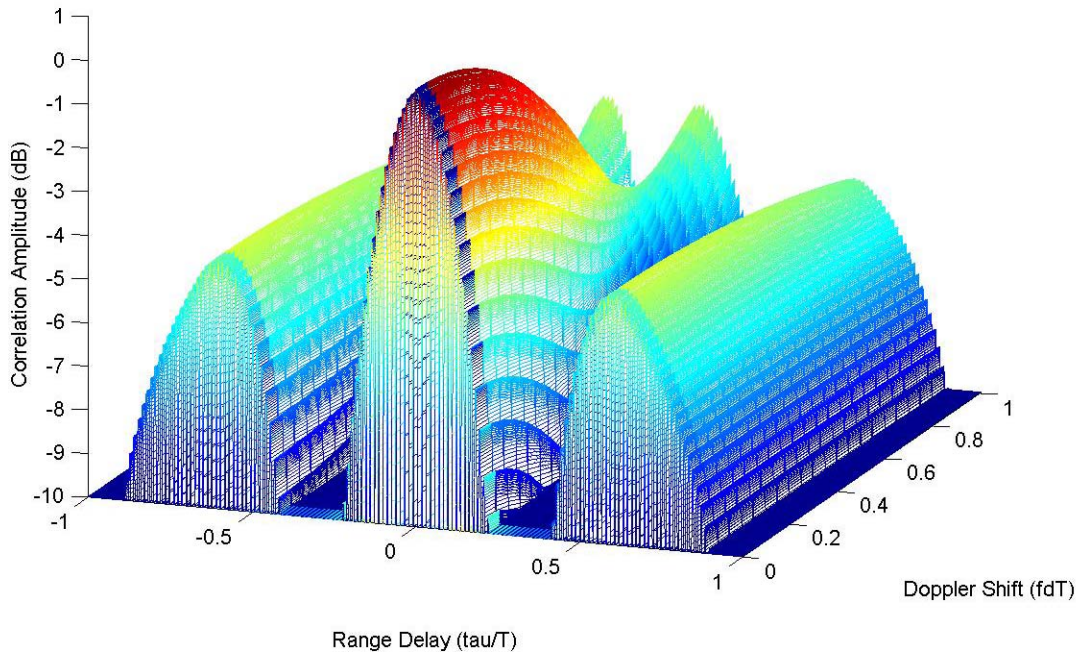
Figure 4.5: Ambiguity diagram for the Frank (14, 14) coded waveform

4.3.3 Welti Code

The Welti code has a much different ambiguity diagram. Welti codes are known for their high mainlobe correlation magnitudes versus sidelobe correlation magnitudes at no Doppler shift [1]. However, their mainlobe correlation magnitude falls off rapidly with increasing Doppler shifts. The final combined metric value for the Welti code is 0.3671, higher (poorer) than the two "best" Frank codes. Figure 4.6 shows the ambiguity diagram for the Welti coded waveform.
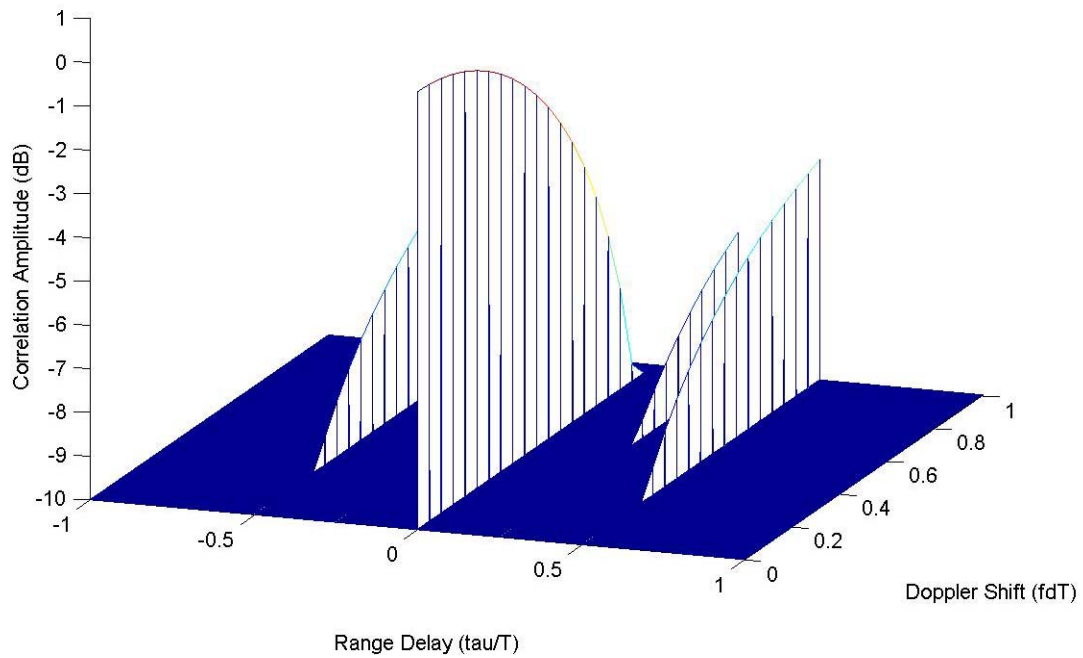
Figure 4.6: Ambiguity diagram for the Welti coded waveform

4.4 Matched Filter

This section describes results from experiments using the matched filter detector. First, a description of how the ROC curves are made for a matched filter detector is presented. Next results from each of the three codes tested and for each Doppler shift level are shown.

4.4.1 Matched Filter Detection

Detection occurs in a matched filter detector when the correlation magnitude exceeds some threshold. The threshold used in all matched filter experiments presented here is computed to yield a P_{fa} equal to 0.01. Figure 4.7 shows the important parts of an example trial. The constant value at the top of the chart is the threshold value. The upper non-constant values are the cross correlation of the test signal plus independent Gaussian noise with the matched filter for the test signal. The lower non-constant curves are the cross correlation of noise with the matched filter for the test signal. The test signal used in this trial is a PM sinusoid with phase shifts of $\pi/2$ and $2\pi/7$ activated at the fifth and seventh period of the carrier wave.
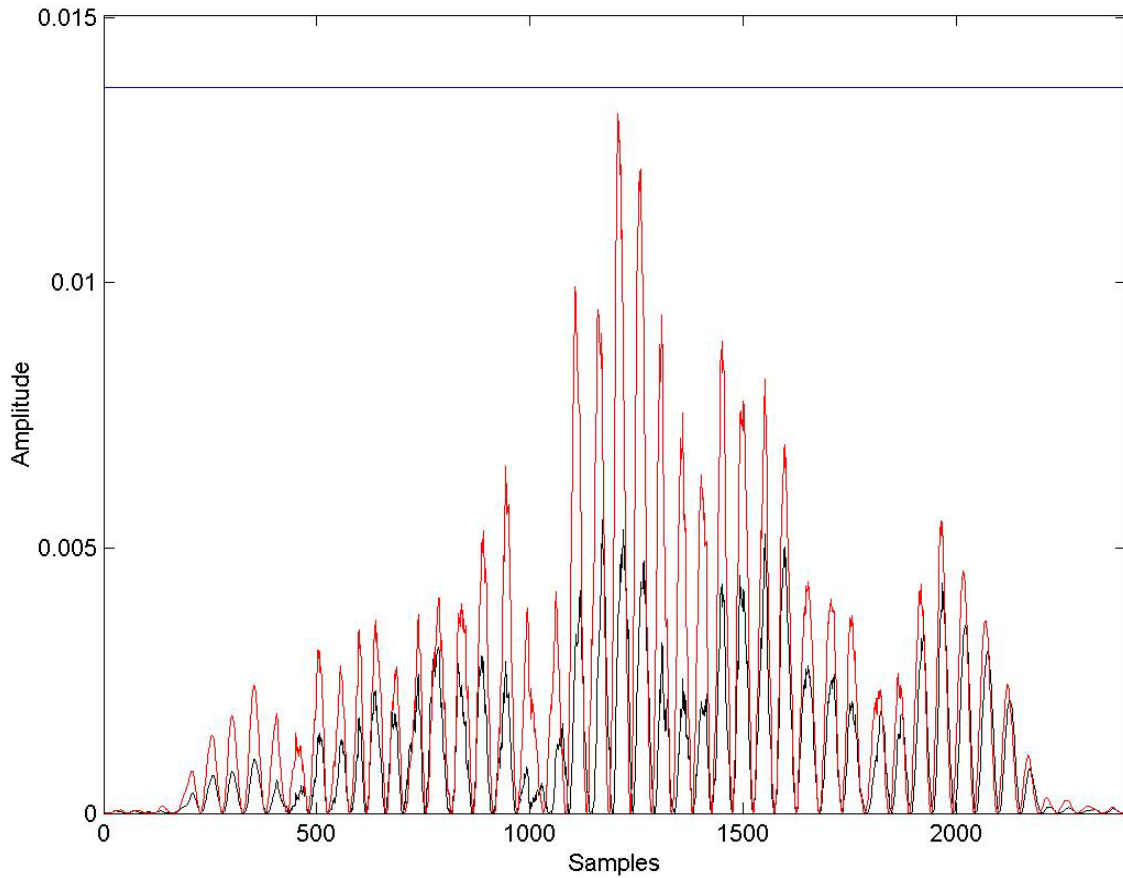
Figure 4.7: One realization of the correlation used to find the probability of detection for a matched filter detector. The lower non-constant values plot a phase modulated sinusoidal waveform consisting of phase shifts of $\mu/2$ and $2\mu/7$ of two-period duration activated at the fifth and seventh period of the wave correlated with independent Gaussian noise. The upper non-constant values are calculated by correlating the phase modulated waveform described above with a scaled waveform plus independent Gaussian noise, where scaling enables variation of the signal-to-noise ratio. The constant value plots a threshold set as the peak value of the unit amplitude waveform correlated with independent Gaussian noise such that there is one false alarm per 100 realizations and thus a probability of false alarm of 0.01. The displayed realization is not a detection because none of the correlation magnitudes exceeds the threshold.

Figure 4.8 shows the ROC curve created using twenty experiments with different SNRs and 100 replications per SNR.
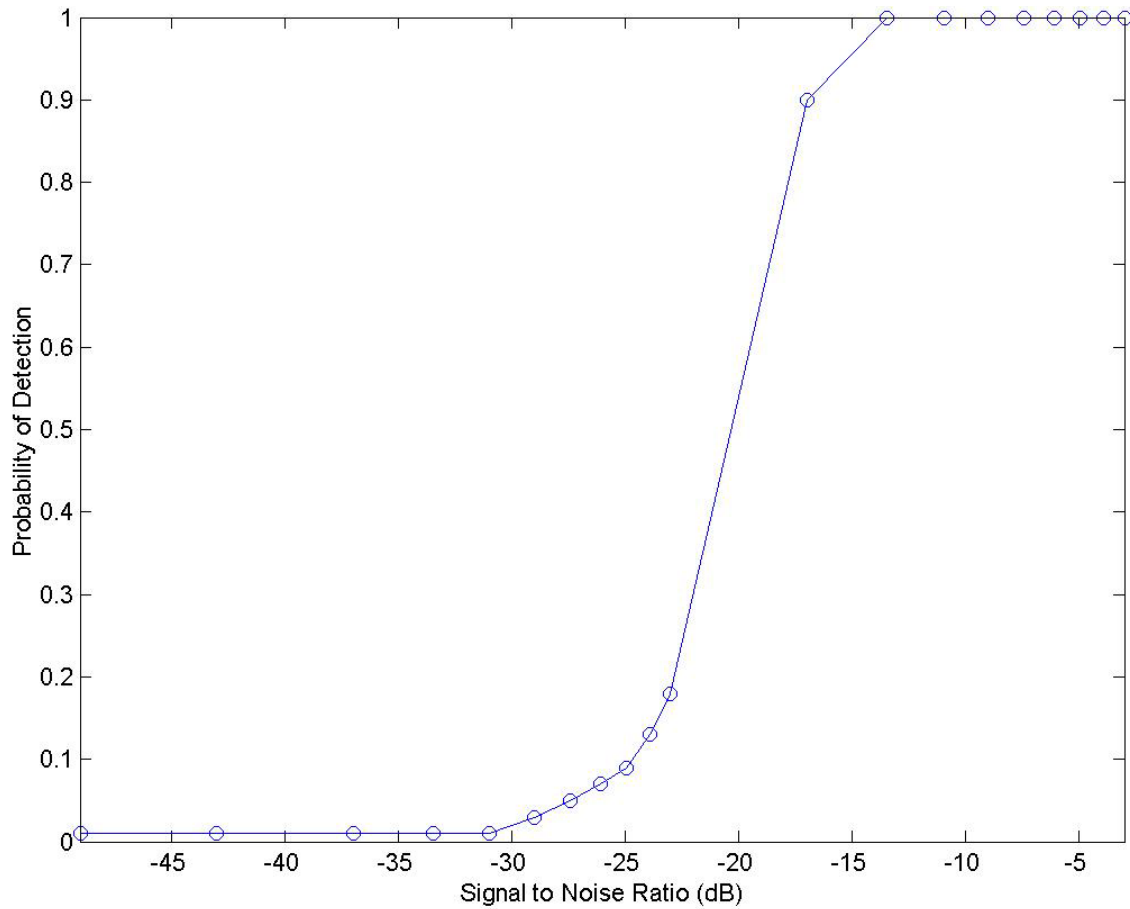
Figure 4.8: ROC curve for a matched filter. Each point is proportional to the number of detections found as illustrated in Figure 4.7. The signal to noise ratio is varied by increasing the amplitude of the waveform. Note that this ROC curve achieves 100% detection at a much lower signal-to-noise ratio than the square-law detector of Figure 4.2.

4.4.2 Frank (13, 13)

The results of the experiments run on the Frank (13, 13) coded waveform are seen in Figure 4.9. This plot is a conglomeration of numerous ROC curves with the received signal shifted by various Doppler levels. The trials and detection criteria are the same as

listed above. This plot shows the degradation that the Frank (13, 13) code suffers at increasing Doppler shift values.
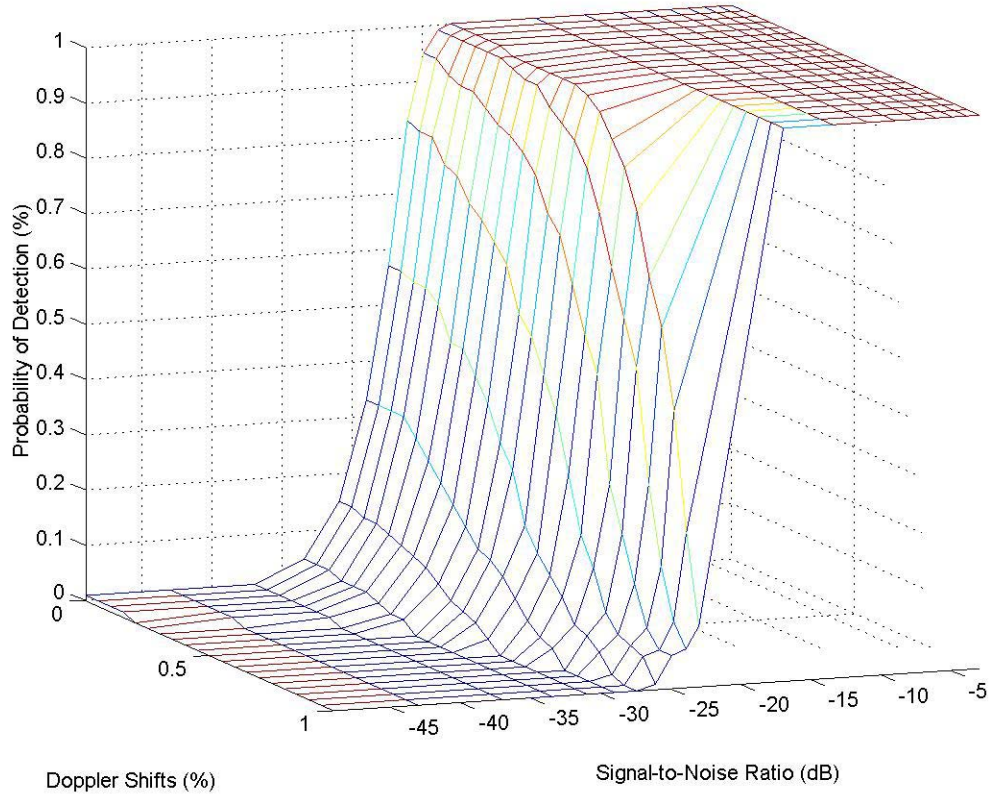
Figure 4.9: ROC curves for Frank (13, 13) coded waveforms across Doppler shift values.

To better view Doppler shift effects on the detection of a Frank (13, 13) coded waveform using a matched filter detector, Figure 4.10 shows three ROC curves for the no Doppler shift, 0.5 Doppler shift, and 1 Doppler shift cases. Data points marked by a 'o' are the non-shifted ROC curve, points marked by a '+' are for the 0.5 Doppler shifted ROC curve, and those marked by 'x' are for the 1 Doppler shifted ROC curve. This figure illustrates how Doppler shift effects the matched filter detector system. However, at peak

Doppler shift of one, the matched filter detects the incoming signal 100% of the time using at 11 dB less SNR than the square-law detector.
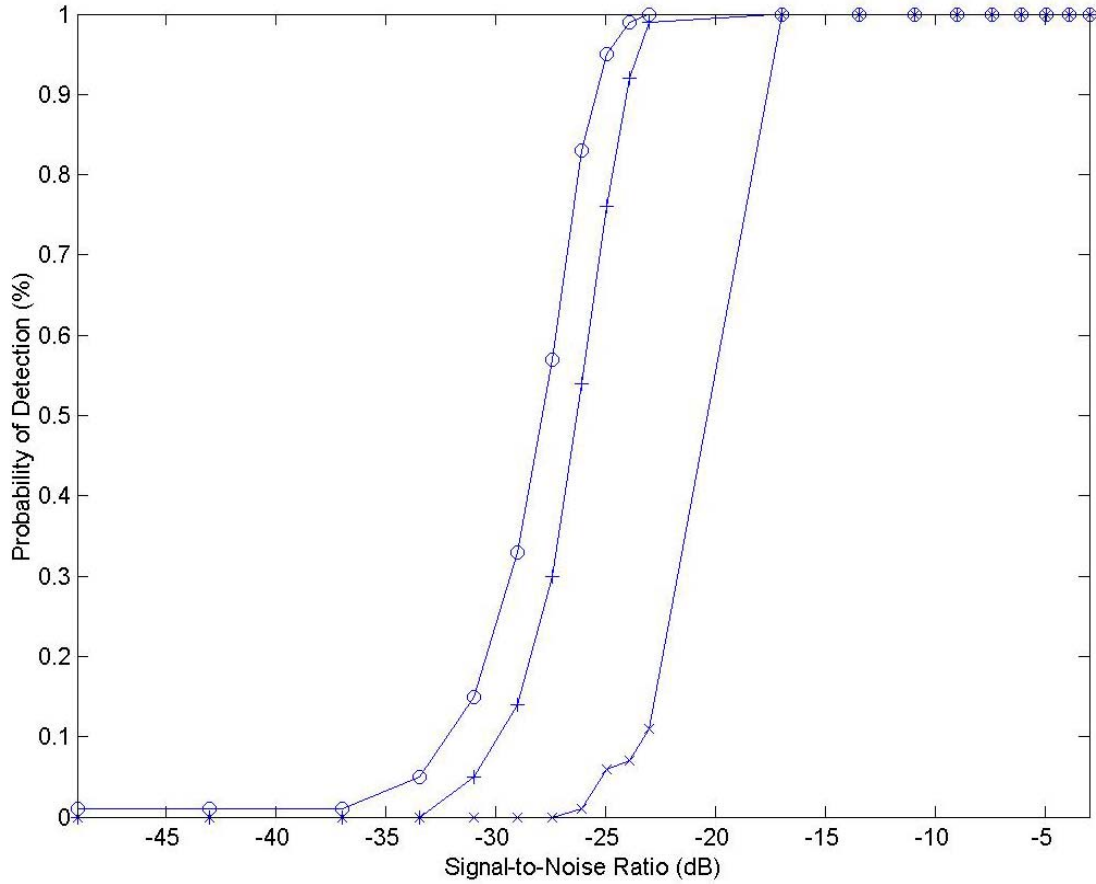
Figure 4.10: ROC curves for a Frank (13, 13) coded waveform on a matched filter detector at different Doppler shift values. The far left curve with the '○' data points is the ROC curve with no Doppler shift. The middle curve with '+' data points is the ROC curve with 0.5 Doppler shift. The far right curve with the 'x' data points is the ROC curve with 1 Doppler shift. Even with the degrading effects of Doppler in full force, the matched filter still detects the Frank (13, 13) coded waveform better than the square-law detector.

4.4.3 Frank (14, 14)

The results from the experiments on the Frank (14, 14) coded waveform are seen in Figure 4.11. This figure plots the ROC curves in the same manner as Figure 4.10. Note that the ROC curves for the matched filter detection of the Frank (14, 14) coded waveform are very similar to the ROC curves found in Figure 4.10.
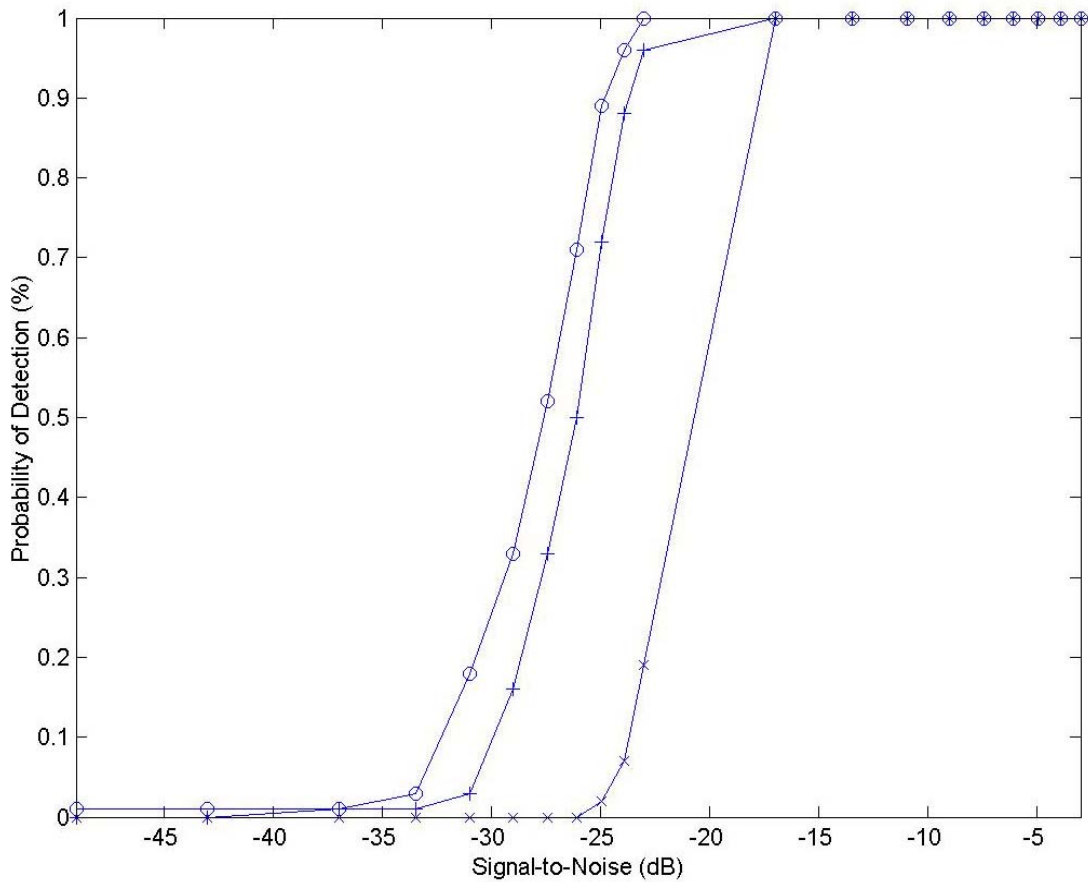
Figure 4.11: ROC curves for a Frank (14, 14) coded waveform on a matched filter detector at different Doppler shift values. The far left curve with the 'o' data points is the ROC curve with no Doppler shift. The middle curve with '+' data points is the ROC curve with 0.5 Doppler shift. The far left curve with the 'x' data points is the ROC curve with 1 Doppler shift. Note the similarities between the Frank 13, 13 curves from Figure 4.10 and Frank (14, 14) curves of this figure.

57

4.4.4 Welti

Results from experiments using Welti coded waveforms are presented in Figure 4.12 which shows the ROC curves for the matched filter detector. Note that the difference between the SNR values at which each of the codes reaches 100% detection from no Doppler to full Doppler shift is approximately equal at 7 dB.
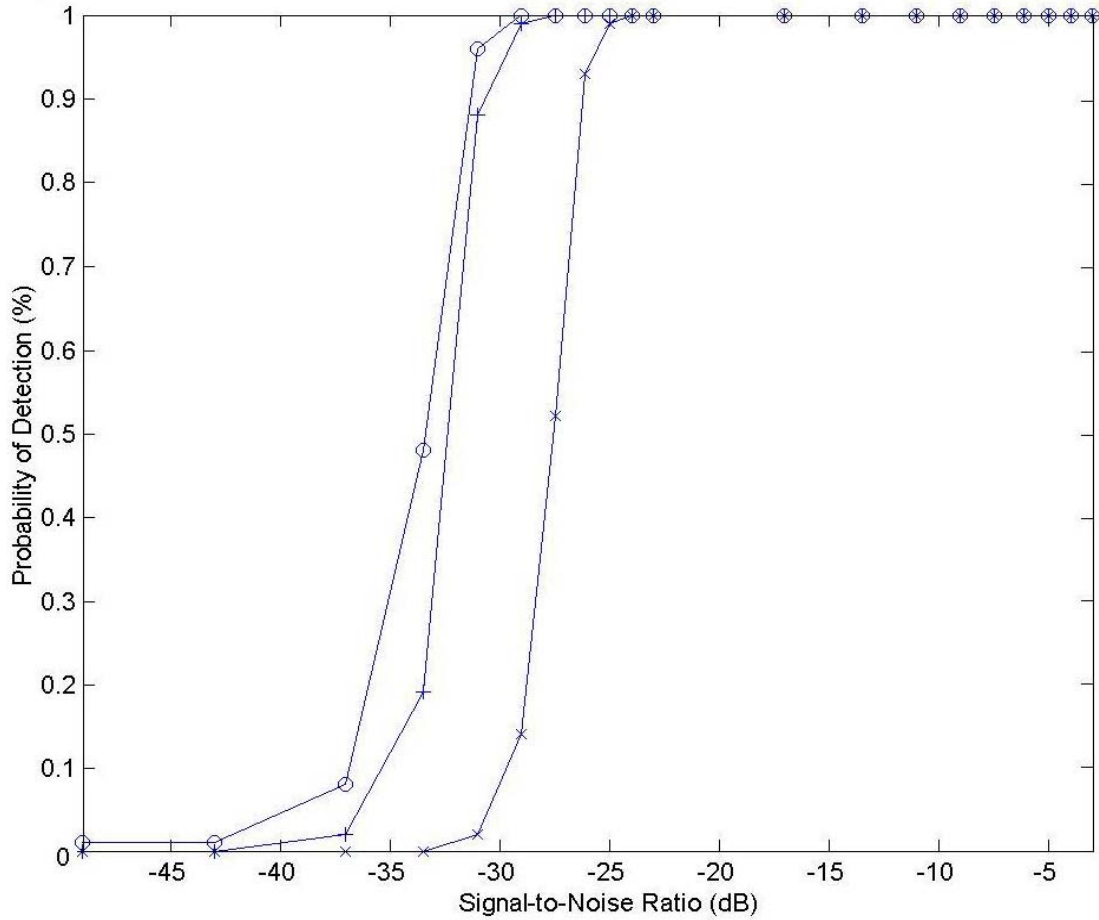
Figure 4.12: ROC curves for a Welti coded waveform on a matched filter detector at
different Doppler shift values. The far left curve with the 'o' data points is
the ROC curve with no Doppler shift. The middle curve with '+' data
points is the ROC curve with 0.5 Doppler shift. The far left curve with the
'x' data points is the ROC curve with 1 Doppler shift. This plot shows the
Welti coded waveforms to have a much superior performance over the two
Frank coded waveforms tested.

4.5   Brown Symbols

Another set of waveforms that have recently been developed are named Brown Symbols.

The ambiguity diagrams, one of which is shown in Figure 4.13, as well as the metric

values described earlier suggest that these codes may be good candidates for further

research. The combined metric value for the Brown symbol seen in Figure 4.13 is 0.2417, better (lower) than the two best Frank codes and the Welti code.
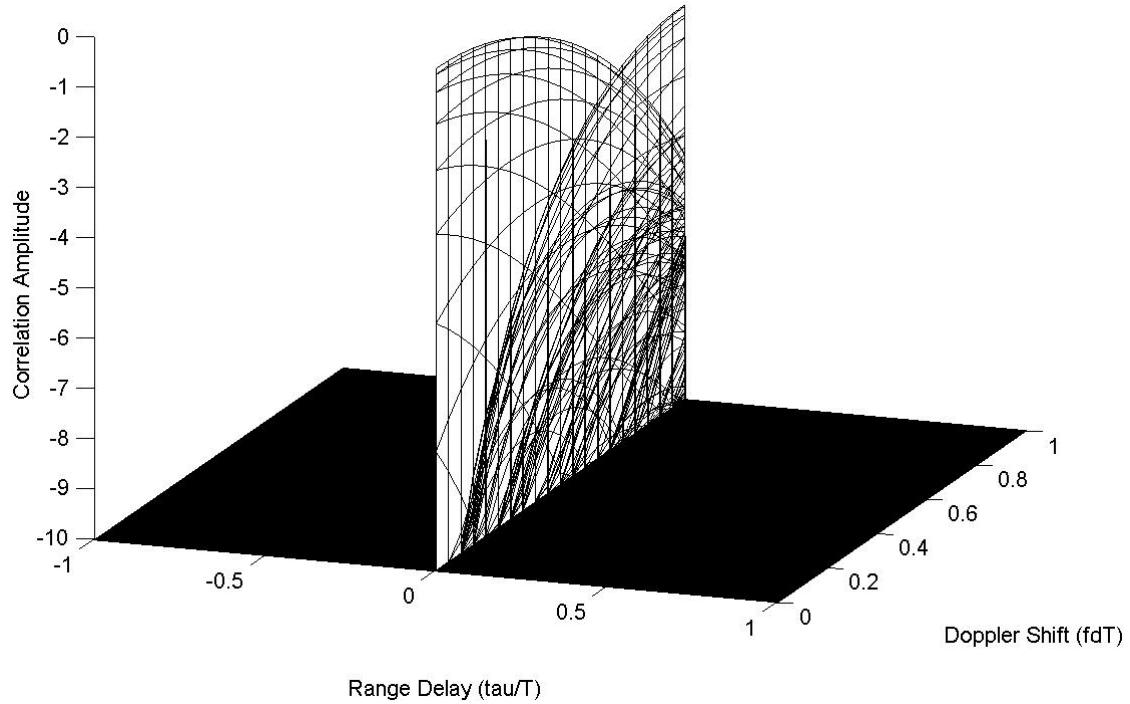
Figure 4.13: Ambiguity diagram for a Brown symbol

The final chapter gives conclusions to the experiments presented in this chapter as well as suggestions for further research.

Chapter 5 Conclusions

This chapter contains a discussion of the conclusions drawn from the results presented in Chapter 4 as well as suggestions for possible further research, and a brief discussion of the thesis contributions.

5.1   Conclusions from Results

Analysis of the results seen in Chapter 4 leads to the conclusion that for the Frank coded waveforms, detectors, and metrics used in testing, the Welti and Frank coded waveforms have similar performance. Test on all three waveforms yielded similar degradation at increasing Doppler shift levels. Therefore, there is no discernable advantage for using either of the Frank codes tested.

5.2   Further Research

A number of possible research avenues remain unexplored. Clearly there are an infinite number of Frank codes. Only 69 Frank codes were evaluated by the metrics, and only two were tested for detection; their marginal performance does not provide any reason to recommend using Frank codes in radar systems. The two codes tested are just a small subset of the total number of possible Frank codes, any one of which could give better performance. Also, combining the rows of a Frank code matrix into one vector may yield better results [3].

Frank codes are but one of a number of radar pulse modulation schemes. Other modulation schemes may prove to provide increased capabilities over the Welti codes according to the criteria tested. In particular, a new radar waveform coding technique, known unofficially as 'Brown Symbols,' may provide much improved performance.

There are numerous other radar waveform detectors that were not investigated as part of this research. Frank codes may prove more resistant using these other types of detectors than the Welti code. Some of these possible detectors include the delay and multiply, 4th law, and wideband crystal video detectors.

Finally, radar waveform filters have been developed that reduce a particular waveform's exploitation by certain detectors. In particular, the SEI proprietary filter used in the 1997 FAMU/FSU study [1] could be used. Different codes could be applied to different waveforms, the waveforms could be filtered, and then tested against several of the detectors mentioned above.

5.3   Thesis Contributions

This thesis tested detection performance differences between two certain Frank and Welti coded radar waveforms. The conclusions from the tests indicate that for the Frank codes tested, the Welti code remained the superior performer. These results are surprising due to reported resistance of Frank codes to Doppler shifts.

The process by which these conclusions were made will allow future researchers to continue this type of study much more efficiently. The MATLAB files used to gather data and run experiments are found in Appendix B. Each of the suggested further research ideas listed above can be completed with minimal changes to the files seen in Appendix B and to the methodology listed in Chapter 3.

Appendix A

This appendix has the ROC curves for the square-law detector and different waveforms. The first is the Frank 14,14 coded waveform, the second is the Welti coded waveform, and the last is a simple carrier sine wave.
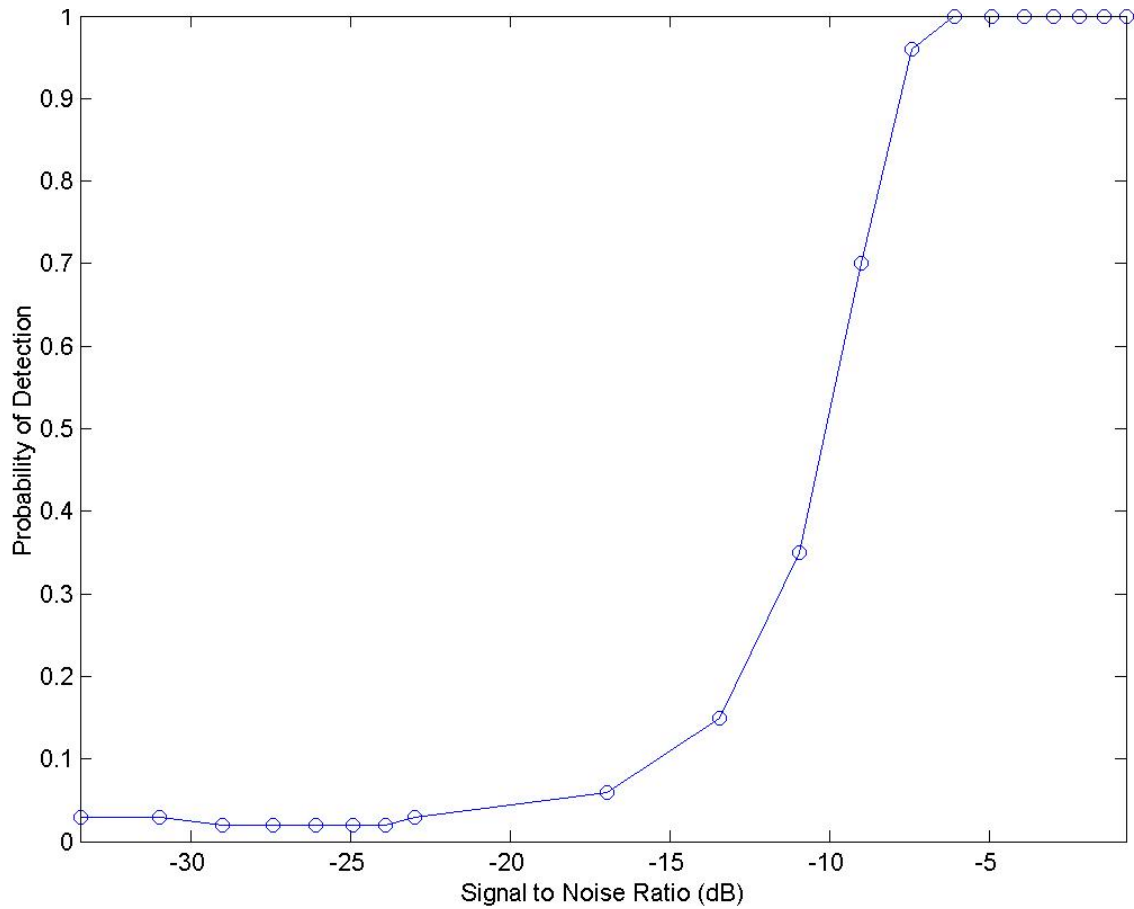
Figure A.A.1: ROC curve for square-law detection of the Frank 14,14 coded waveform.
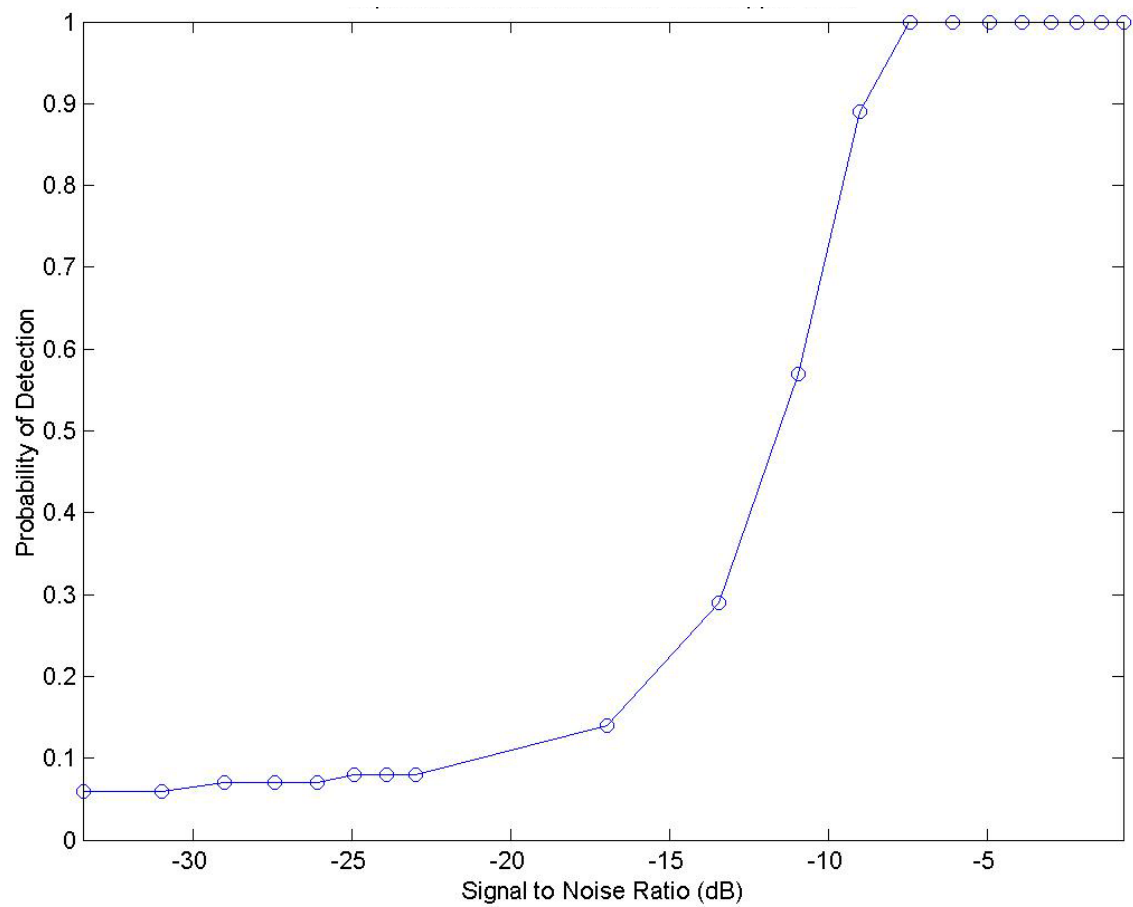
Figure A.A.2: ROC curve for square-law detection of the Welti coded waveform.
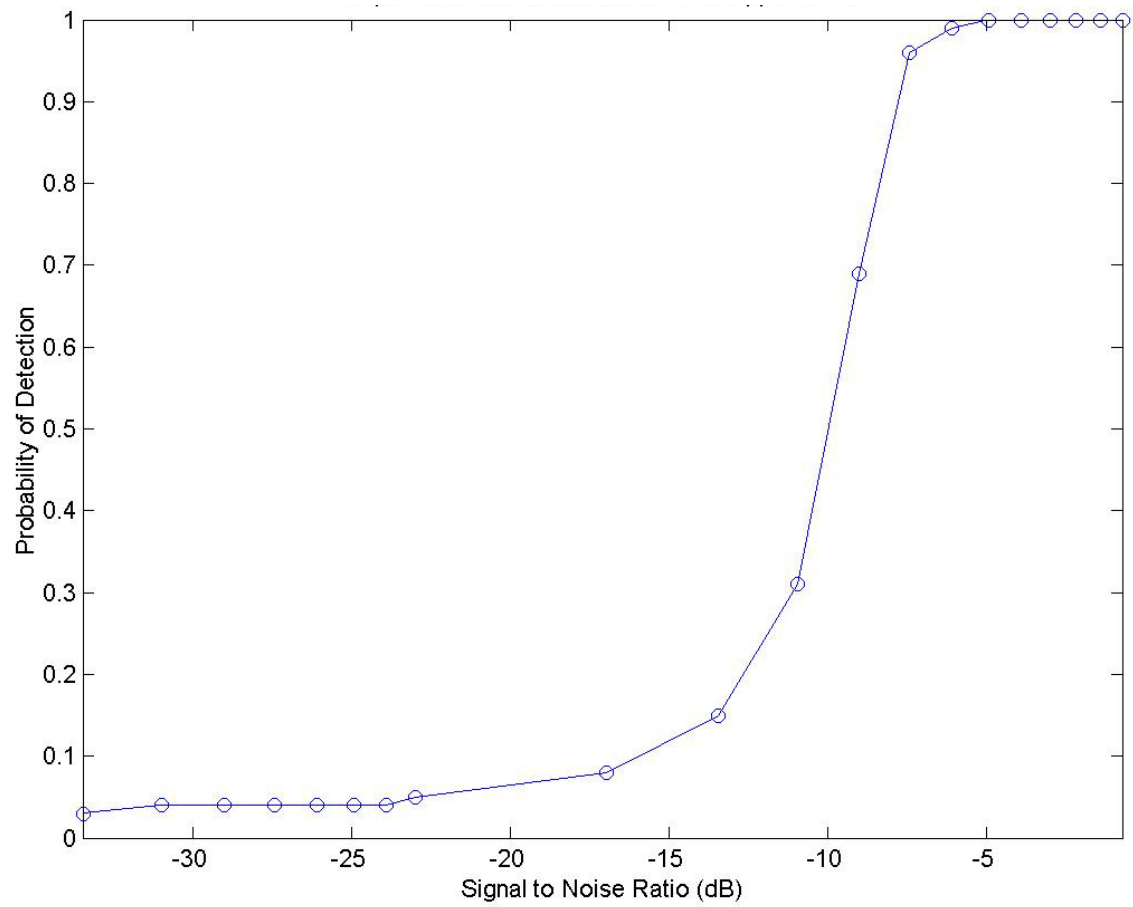
Figure A.A.3: ROC curve for square-law detection of a simple sine wave.

Appendix B

This appendix contains the MATLAB files used in this research. All values are set according to the last simulation run.

Frank.m: Creates a Frank coded waveform


```
%  Lt. Geoffrey G. Bowman
%  Air Force Institute of Technology
%  Thesis Research
%  24 July 2002


%%%%%%%%%%%%%%%%%%%%%%%%%%%%%%%%%%%%%%%%%%%%%%%%%%%%%%%%%%%
%                                                        %
%  This code is an attempt to enter a Frank polyphase    %
%  code into MATLAB so that it can be used in conjunction %
%  with the SEI Inc. proprietary filter software.        %
%                                                        %
%%%%%%%%%%%%%%%%%%%%%%%%%%%%%%%%%%%%%%%%%%%%%%%%%%%%%%%%%%%




% Frank code with M = length

codelength = 13;
jay = sqrt(-1);
wav = {codelength};
phase = 360/codelength;
k = 0;
zeropad = 1;
samperper = 192;
chiplength = 1;                                    %Indicates a
phase change every 1/16th of a period
fs=12 * samperper;
%fs is samples.  This value ensures 192 samples per period of the
carrier.
t=(1/(fs*1E6))*[1:codelength];
carrier=sin(2*pi*12E6*t);
wavetotal = [];
waves = [];
wavetotals = [];
for j=1:codelength
    for i=1:codelength
        wav{i,j} = (mod((k*(i - 1) * phase), 360));
    end
    k = k + 1;
end

codetotal = [];
codetotals = [];
ratiostotal = [];
for j = 1:codelength
    wave = [];
    for i = 1:codelength
        wave = [wave, wav{j,i}];
    end
    codetotal = [[codetotal];[wave]];
end

for j=1:codelength
    for i=1:codelength
        codetotal(i,j) = ((codetotal(i,j)*2*pi)/360);
    end
end
```


68

```matlab
wavee = [];
for k = 1:codelength
    wavee = [];
    for i = 1:codelength
        waves = [];
        for j = 1:(chiplength * samperper)
            waves = [waves,codetotal(k,i)];
        end
        wavee = [wavee, waves];
    end
    codetotals = [[codetotals];[wavee]];
end

codetotals =
[zeros(codelength,zeropad*codelength*chiplength*samperper)...
        codetotals
zeros(codelength,zeropad*codelength*chiplength*samperper)];
%codetotals = [zeros(codelength,576) codetotal zeros(codelength,576)];

wavefor = [];
t=(1/(fs*1E6))*[1:length(codetotals)];
carrier=sin(2*pi*12E6*t);

for row = 1:codelength
    wavefor = [];
    for i = 1:length(codetotals)
        wavefor = [wavefor sin(2*pi*12E6*t(i)+codetotals(row,i))];
    end
    wavetotals = [[wavetotals];[wavefor]];
end

%wavetotals = codetotals;


%for i = 1:codelength
%    figure
%    plot(wavetotals(i,:))
%    title(i)
%    xlabel('Time')
%    ylabel('Amplitude')
%end


%for j = 1:length(codetotal)
%    wave = [];
%    for i = 1:codelength
%        wave = [wave, exp(jay*codetotal(i,j))];
%    end
%    wavetotal = [[wavetotal];[wave]];
%end
%wavetotals = wavetotal';

%wavetotals = [zeros(codelength,576) wavetotal zeros(codelength,576)];

%for j = 1:codelength
%    wavetotal(j,:) = carrier.*wavetotal(j,:);
%end
```

Welti1k.m: Creates a Welti code

```
%%%%%%%%%%%%%%%%%%%%%%%%%%%%%%%%%%%%%%%%%%%%%%%%%%%%%%%%%%%%%%%%%%%%%%%%
%%%%%%%%%%%%%%%%%%%%%   Welti code generator   %%%%%%%%%%%%%%%%%%%%%%%%%
%%%%%%%%%%%%%%%%%%%%%%%%%%%%%%%%%%%%%%%%%%%%%%%%%%%%%%%%%%%%%%%%%%%%%%%%
%  L -- number of chips in the Golay coded pair
%        (must be a power of two)
%  a, b  -- Welti codes
%  awav, bwav --  Welti codes sampled  8 times per chip and mulitplied
%                      by a 12 MHz carrier (192 MHz sample
frequency).
%%%%%%%%%%%%%%%%%%%%%%%%%%%%%%%%%%%%%%%%%%%%%%%%%%%%%%%%%%%%%%%%%%%%%%%%

L=1024;

%%%%%%%%%%%%%%%%%%%%%%%%%%%%%%%%%%%%%%%%%%%%%%%%%%%%%%%%%%%%%%%%%%%%%%%%
%  Initial codes
%%%%%%%%%%%%%%%%%%%%%%%%%%%%%%%%%%%%%%%%%%%%%%%%%%%%%%%%%%%%%%%%%%%%%%%%

a=[1,1];
b=[-1,1];   %old is b=[-1,1];

%%%%%%%%%%%%%%%%%%%%%%%%%%%%%%%%%%%%%%%%%%%%%%%%%%%%%%%%%%%%%%%%%%%%%%%%
%  Generate codes
%%%%%%%%%%%%%%%%%%%%%%%%%%%%%%%%%%%%%%%%%%%%%%%%%%%%%%%%%%%%%%%%%%%%%%%%

n=log2(L);
for i=2:n,
    c=[a,-1.*b];
    d=[a,b];
    a=c;
    b=d;
end

fs=192;                                          %%%SEI%%%

clear i
clear c
clear d
clear L


%Modified by Lt Geoffrey G. Bowman 12 Aug. 2002
awav = a;
bwav = b;
wavetotals = awav;
```

70

Newambig.m: Creates an ambiguity diagram

```
%%%%%%%%%%%%%%%%%%%%%%%%%%%%%%%%%%%%%%%%%%%%%%%%%%%%%%%%%
%       Ambiguity Diagram Generator                    %
%                                                       %
%  This program assumes an input waveform (wave)        %
%  and plots the Ambiguity diagram.  The time scale     %
%  is normalized and varies as -1 < tau/T < 1 where     %
%  tau is the range delay and T is the pulse length     %
%  the frequency scale is the Doppler shift in          %
%  discrete intervals and varies as 0 < fdT < 1         %
%  such that the doppler shift varies up to 1/T         %
%  This range of Doppler is consistent with Baden,      %
%  "Optimal Peak Sidelobe Filters for Biphase Pulse     %
%  Compression", Proc. 1990 Inter. Radar Conf., May '90 %
%%%%%%%%%%%%%%%%%%%%%%%%%%%%%%%%%%%%%%%%%%%%%%%%%%%%%%%%%


%%%%%%%%%%%%%%%%%%%%%%%%%%%%%%%%%%%%%%%%%%%%%%%%%%%%%%%%%
%  This version is set up to run with the Frank.m file  %
%  that makes a Frank code of length = codelength and   %
%  modulates it on a 12 GHz carrier wave.               %
%%%%%%%%%%%%%%%%%%%%%%%%%%%%%%%%%%%%%%%%%%%%%%%%%%%%%%%%%

%clear

%frank


whitebg('w')

jay=sqrt(-1);

mlcmetricvalues = [];
mlslratiometricvalues = [];
mlwmetricvalues = [];
%%%%%%%%%%%%%%%%%%%%%%%%%%%%%%%%%%%%%%%%%%%%%%%%%%%%%%%%%
%                                                      %
%  Enter row of Frank code to be evaluated in as row   %
%                                                      %
%%%%%%%%%%%%%%%%%%%%%%%%%%%%%%%%%%%%%%%%%%%%%%%%%%%%%%%%%

row = 1;
%arow = 33;
%brow = 66;
%for row = 1:codelength

N=length(wavetotals(row,:));
%delta = pi/10240;                       %numerical value used in
Ambig.m
delta=pi/(10*N);                         %original delta used in sei
software

%delta=(1267/2100)*pi/(10*N);            %For Frank 1313, delta such
that the peak at top doppler shift is .5 of the peak at no doppler shift
%delta=(1267/2100)*pi/(10*N);            %For Frank 1414, delta such
that the peak at top doppler shift is .5 of the peak at no doppler shift
%delta=(1267/2100)*pi/(10*N);            %For Frank 1515, delta such
that the peak at top doppler shift is .5 of the peak at no doppler shift
%
```

```
NN=21;          % 21 different doppler shifts in increments of i/((NN-1)Tau)
y=[0:NN-1]/(NN-1);
x=[-(N-1):(N-1)]/(N-1);


for j=1:NN
    for i=1:N
        awavee(i)=wavetotals(row,i)*exp(-jay*delta*(i-1)*(j-1));
%        awavee(i)=wavetotals(arow,i)*exp(-jay*delta*(i-1)*(j-1));
%        bwavee(i)=wavetotals(brow,i)*exp(-jay*delta*(i-1)*(j-1));
    end

    apsi(j,:)=xcorr(wavetotals(row,:),awavee)/N;
%     apsi(j,:)=xcorr(wavetotals(arow,:),awavee)/N;
%     bpsi(j,:)=xcorr(wavetotals(brow,:),bwavee)/N;

%     psi(j,:)=abs(apsi(j,:)+bpsi(j,:));
    psi(j,:)=abs(apsi(j,:));
end


z = psi./max(max(psi));
showpictures
constancy
mlslratio
%mlwidths
mlcmetricvalues = [mlcmetricvalues; finalmlcmetric];
mlslratiometricvalues = [mlslratiometricvalues; finalmlslmetric];
%mlwmetricvalues = [mlwmetricvalues; finalmlwmetric];
%end
mlcmetricvalues
mlslratiometricvalues
%mlwmetricvalues
```

Constancy.m: Calculates the mainlobe constancy metric

```
%%%%%%%%%%%%%%%%%%%%%%%%%%%%%%%%%%%%%%%%%%%%%%%%%%%%%%%%%%%%%%%%%%%%%%%%%%%%
%
%    This matlab file will determine the constancy of the mainlobe of a
%    radar waveform.  Its purpose in this research is to help determine
%    which Frank codes to research further.
%    Written By:  Lt. Geoffrey  G. Bowman
%    Written on:  23 October 2002
%
%%%%%%%%%%%%%%%%%%%%%%%%%%%%%%%%%%%%%%%%%%%%%%%%%%%%%%%%%%%%%%%%%%%%%%%%%%%%


%%%%%%%%%%%%%%%%%%%%%%%%%%%%%%%%%%%%%%%%%%%%%%%%%%%%%%%%%%%%%%%%%%%%%%%%%%%%
%
%    First determine the mainlobe peak.  The matlab file Frank.m will
%    create a matrix of values to include every Frank code of length
%    codelength.  An ambiguity diagram is then created for each of these
%    codes with the file newambig.m.  The final values for the ambiguity
%    diagram are contained in the z matrix, a 21 row, 2 * codelength + 1
%    column matrix of values.  The peak mainlobe values are contained in
%    center column, coincidentally enough the column equal to codelength.
%    The standard deviation of these values will be the final metric
%    value of this file.  This is a lower better metric in that a value
%    of 0 would indicate an entirely flat peak mainlobe.
%
%%%%%%%%%%%%%%%%%%%%%%%%%%%%%%%%%%%%%%%%%%%%%%%%%%%%%%%%%%%%%%%%%%%%%%%%%%%%

corrlength = length(psi(row,:));
%The length of the correlation
corrcent = (corrlength+1)/2;
%The center value of the correlation (Its peak)


peakmainlobe = z(:,corrcent);
%The peak mainlobe column

finalmlcmetric = std(peakmainlobe);
%The unscaled metric value
```

Mlslratio.m: Calculates the sidelobe to mainlobe ratio metric

```
%%%%%%%%%%%%%%%%%%%%%%%%%%%%%%%%%%%%%%%%%%%%%%%%%%%%%%%%%%%%%%%%%%%%%%%%%%
%
%    This MATLAB file determines the mainlobe to sidelobe levels.  A low
%    level of sidelobes compared to mainlobe indicates a better code for
%    the purposes of this research.
%    Written by: Lt. Geoffrey G. Bowman
%    Written on: 24 October, 2002
%
%%%%%%%%%%%%%%%%%%%%%%%%%%%%%%%%%%%%%%%%%%%%%%%%%%%%%%%%%%%%%%%%%%%%%%%%%%


%%%%%%%%%%%%%%%%%%%%%%%%%%%%%%%%%%%%%%%%%%%%%%%%%%%%%%%%%%%%%%%%%%%%%%%%%%
%
%    The metric for the mainlobe to sidlobe value will be a ratio.  This
%    ratio is weighted using the softmax function so that any code that
%    yeilds a higher sidelobe than mainlobe value will give a greater
%    metric value in this lower better metric.  The mainlobe for this
%    research is defined as the 3dB range from the max power level at a
%    Doppler shift of 0 (autocorrelation function).  The MATLAB code is
%    set up in such a way that the 3dB point will rarely if ever fall on
%    an actual data point.  Therefore the actual mainlobe will be from
%    peak power point to the last data value before the 3dB point.  This
%    should allow for a greater mainlobe value than sidelobe value even
%    in general cases.
%
%%%%%%%%%%%%%%%%%%%%%%%%%%%%%%%%%%%%%%%%%%%%%%%%%%%%%%%%%%%%%%%%%%%%%%%%%%


%%%%%%%%%%%%%%%%%%%%%%%%%%%%%%%%%%%%%%%%%%%%%%%%%%%%%%%%%%%%%%%%%%%%%%%%%%
%
%    Part 1:  Find the extent of the mainlobe.  The ambiguity diagram is
%    normalized such that the peak power values is 1 and the minimum
%    power level is 0.  This means that logically the half power level
%    is at 0.5.  This section will find the nearest data point at or
%    after the half power level.
%
%%%%%%%%%%%%%%%%%%%%%%%%%%%%%%%%%%%%%%%%%%%%%%%%%%%%%%%%%%%%%%%%%%%%%%%%%%

%corrlength = length(psi(row,:));
%The length of the correlation
corrlength = length(psi);
corrcent = (corrlength+1)/2;
%The center value of the correlation (Its peak)
mlvalue = 1;
%This variable is used to find the length of the mainlobe.
maxml = corrcent;
%This is the array index of the maximum data part of the mainlobe
while(mlvalue >= .5)
%This loop finds the data point where the mainlobe equals .5
    mlvalue = z(1,maxml);
%
    maxml = maxml + 1;
%
end
%
if (mlvalue < .5)
%If the stop value was less than .5 then back up 2 to the correct
%mainlobe range
```

```
    maxml = maxml - 2;
%
else
%If the stop value was equal to .5 then back up 1 to the correct
%mainlobe range
    maxml = maxml - 1;
%
end
%
minml = corrcent - (maxml - corrcent);
%The minimum of the mainlobe range will be the same distance from the
%peak as the maximum.  This variable represents this.

%


%
%%%%%%%%%%%%%%%%%%%%%%%%%%%%%%%%%%%%%%%%%%%%%%%%%%%%%%%%%%%%%%%%%%%%%%%%%
%
%    Part 2:  Now that the mainlobe is seperated from the sidelobes,
%    the mainlobe to sidelobe ratios must be computed.  This part will
%    compute this ratio.  The peak mainlobe and sidelobe values at each
%    doppler shift will be found.
%
%%%%%%%%%%%%%%%%%%%%%%%%%%%%%%%%%%%%%%%%%%%%%%%%%%%%%%%%%%%%%%%%%%%%%%%%%


maxmlvalue = [];
%This is the maximum value of the mainlobe at the particular doppler
%shift
maxslvalue = [];
%This is the maximum value of the sidelobe at the particular doppler
%shift
mlslratios = [];
%This is the ratio of peak mainlobe and sidelobe values
z = psi;
%
for i = 1:20
%
%for i = 1:21
%1 to 21 for proper cases (mainlobe doesn't go all the way to 0)

%1 t0 20 for improper cases (mainlobe does go to 0)

%

%This loop finds the maximum mainlobe and sidelobe values for each of
%the doppler shifts.
    mlvalues = z(i,minml:maxml);
%
    maxmlvalue = [maxmlvalue, max(mlvalues)];
%
    slvalues = z(i,1:(minml-1));
%
    maxslvalue = [maxslvalue, max(slvalues)];
%
end
%


%
maxslvalue;
%
maxmlvalue;
%
```

```
mlslratios = maxslvalue ./ maxmlvalue;
%This array holds the actual ratio values.  A greater than 1 value
%indicates

%the sidelobe is greater than the mainlobe at a particular value.

%

%
%%%%%%%%%%%%%%%%%%%%%%%%%%%%%%%%%%%%%%%%%%%%%%%%%%%%%%%%%%%%%%%%%%%%%%%%%%
%
%    Part 3:  The softmax function.  This part will apply the softmax
%    function to the ratios calculated in part 2.  The softmax function
%    will make ratios greater than one recieve the majority of the
%    weight while values less than one will reciev significantly less.
%    The seperating boundary is based on a sigmoid function whose
%    rigidness varies with the value of the constant k.
%
%%%%%%%%%%%%%%%%%%%%%%%%%%%%%%%%%%%%%%%%%%%%%%%%%%%%%%%%%%%%%%%%%%%%%%%%%%


k = 10;
%k is a constant used in the softmax function.  A higher k value means a
%more rigid sigmoid function

%
N = 0;
%N is a constant used in the softmax function
n = 21;
%n is the number of doppler shifts
temp = 0;
for i = 1:20
%for i = 1:21
    N = N + (1 + exp(-k * (mlslratios(i) - 1))) ^ -1;
end
N = N ^ -1;

for i = 1:20
%for i = 1:21
    temp = temp+N*(1+exp(-k*(mlslratios(i)-1)))^(-1)*mlslratios(i);
end

finalmlslmetric = 1/n * temp;

%finalmlslmetric = mean(mlslratios);
```

Showpictures.m: Displays a 3-D plot of the ambiguity diagram values

```
%  mesh produces a mesh surface

zshift = z+1e-6;
zshift = 10*log10(zshift);
for i = 1:length(zshift)
    for j = 1:21
        if zshift(j,i)<-10
            zshift(j,i) = -10;
        end
    end
end



figure;
mesh(x,y,zshift);
view(-340,20);
map=[0 0 0];
colormap(map);
grid
xlabel('Range Delay (tau/T)');
ylabel('Doppler Shift (fdT)');
zlabel('Correlation magnitude');
title(row);
axis([-1 1 0 1 -10 max(max(zshift))])
v = axis;
```

Doppexp.m: Creates the ROC curve for a square-law detector


```
%%%%%%%%%%%%%%%%%%%%%%%%%%%%%%%%%%%%%%%%%%%%%%%%%%%%%%%%%%%%
%                                                         %
%    This file is the master file used for determining the   %
%    effects of Doppler shifts on the square law detector.   %
%    It makes up 100 noise realizations to be used in each   %
%    of the experiments.  This file also varies the amplitude%
%    of the input wave so from 0 to 10 in a logarithmic     %
%    fashion.                                               %
%                                                         %
%%%%%%%%%%%%%%%%%%%%%%%%%%%%%%%%%%%%%%%%%%%%%%%%%%%%%%%%%%%%
wave = ones(1,length(wavetotals(1,:)));
%squarewave used for initialization
realizations = 100;
wave = wavetotals(1,:);
noise = [];
%noise realizations used for probabilities of false alarm and detection

for i = 1:realizations                    %sets the noise array
    noise = [noise;randn(1,length(wave))];
end

samples = 100;                            %Number of samples per period

amp = 0;                                  %amplitude of the waveform



noisepow = noise.^2;

noisepowave = [];                         %power of noise in each interval

noisepowtot = [];
%power of the noise in each interval for every noise sample

periods = floor(length(wave)/samples);
%number of periods in the waveform

noisesort = [];
%the noise sorted used to calculate the threshold value

for i = 1:realizations
    noisepowave = [];
    for j = 1:periods
        noisepowave = [noisepowave, mean(noisepow(i,(samples*(j-
1)+1):j*samples))];
    end
    noisepowtot = [noisepowtot;noisepowave];
    noisesort = [noisesort,noisepowave];
end

noisesort = sort(noisesort);

%threshold1 = noisesort(length(noisesort)-length(noisesort)/(12*10));

%Threshold level set for a probability of false alarm of .1

threshold2 = noisesort(ceil(length(noisesort)-
length(noisesort)/(12*100)));
```

78

```
%Threshold level set for a probability of false alarm of .01
%threshold3 = noisesort(ceil(length(noisesort)-
length(noisesort)/(periods*1000)));
%Threshold level set for a probability of false alarm of .001

%thresholds = [threshold1,threshold2,threshold3];
thresholds = [threshold2];
%threshold = max(noisesort);

%amps =[.03 .04 .05 .06 .07 .08 .09 .1 .2 .3 .4 .5 .6 .7 .8 .9 1 1.1 1.2
1.3];

%All the amplitudes to be tested
amps =[.0000003 .000001 .000003 .00001 .00003 .0001 .0003 .001 .003 .01
.03 .1 .3 1 3 10 30 100 300 1000];      %All the amplitudes to be tested

threshold = 0;
detecttot = [];
detecttotd = [];
for t = 1:length(thresholds)
    threshold = thresholds(t);
for trials = 1:length(amps)
    amp = amps(trials);
    noshift
    detecttot = [detecttot, detect];
%    shift
%    detecttotd = [detecttotd, detectd];
    trials;
end
end
detecttot;
%detecttotd;

sigtono = 10 * log10(amps.^2/2);
figure
plot(sigtono,detecttot(1:20)/realizations)
hold on
plot(sigtono,detecttot(1:20)/realizations,'o')
%plot(sigtono,detecttot(21:40)/realizations)
%plot(sigtono,detecttot(21:40)/realizations,'x')
%plot(sigtono,detecttot(41:60)/realizations)
%plot(sigtono,detecttot(41:60)/realizations,'+')
%plot(sigtono,detecttotd(1:20)/realizations,'-.r')
%plot(sigtono,detecttotd(1:20)/realizations,'or')
%plot(sigtono,detecttotd(21:40)/realizations,'-.r')
%plot(sigtono,detecttotd(21:40)/realizations,'xr')
%plot(sigtono,detecttotd(41:60)/realizations,'-.r')
%plot(sigtono,detecttotd(41:60)/realizations,'+r')

%plot(sigtono,detecttotd/1000,'o')
%plot(sigtono,detecttotd/1000,'-.')
hold off
title('Square Law Detector Curves with Doppler Shift')
xlabel('Signal to Noise Ratio (dB)')
ylabel('Probability of Detection')
axis([10*log10(amps(1)^2/2) 10*log10(amps(length(amps))^2/2) 0 1]);
v = axis;
```

Noshift.m: Calculates detection data for a square-law detector at no Doppler shift

```matlab
%%%%%%%%%%%%%%%%%%%%%%%%%%%%%%%%%%%%%%%%%%%%%%%%%%%%%%%%%%%%%%%%%%%%%%%
%                                                                   %
%    In this example, a simple phase modulated waveform with  %
%    2 pase shifts is used to demonstrate the limited impact  %
%    of Doppler effect on the square law passive detector.    %
%    The frequency of the wave is relative meaning that the   %
%    results from this experiment will not change for         %
%    different frequencies.  This experiment also assumes      %
%    the detector gathers data in sample periods equal to     %
%    the wave period.                                         %
%                                                                   %
%%%%%%%%%%%%%%%%%%%%%%%%%%%%%%%%%%%%%%%%%%%%%%%%%%%%%%%%%%%%%%%%%%%%%%%


%clear



%two = 1/samples*[1:2*samples];          %2 periods worth of values
%four = 1/samples*[1:4*samples];         %4 periods worth of values

%wavec = amp * sin(2*pi*four);           %the carrier waveform
%wave1 = amp * sin(2*pi*two+(pi/2));     %the first modulated waveform
%wave2 = amp * sin(2*pi*two+(2*pi/7));   %the second modulated waveform
%wave = [wavec wave1 wave2 wavec];       %the wave form put togther
wave = amp * wave;

wavepow = wave.^2;                        %the power of the combined
waveform

detect = 0;
nwave = [];
nwavepow = [];

nwavepowavetot = [];
for i = 1:realizations
    nwavepowsort = [];
    nwavepowave = [];
%    nwave = [nwave;noise(i,:)+wave];
    nwavepow = [nwavepow;(noise(i,:)+wave).^2];
    for j = 1:periods
        nwavepowave = [nwavepowave, mean(nwavepow(i,(samples*(j-
1)+1):j*samples)) * ones(1,samples)];
    end
    nwavepowavetot = [nwavepowavetot; nwavepowave];
    if(max(nwavepowavetot(i,:)) >= threshold)
      detect = detect + 1;
    end
%    nwavepowsort = sort(nwavepow(i,:));

end

%figure
%plot(nwavepow(i,:),'-.y')
%hold on
%plot(threshold*ones(1,length(wave)),'.b')
%plot(nwavepowavetot(i,:),'k.')
%hold off
%axis([0 length(wave) 0 20])
```

```
%v = axis;
%detect
```

Shift.m: Calculates detection data for a square-law detector at no Doppler shift

```
%%%%%%%%%%%%%%%%%%%%%%%%%%%%%%%%%%%%%%%%%%%%%%%%%%%%%%%%%%%%%%%%%
%                                                             %
%    This file uses the same phase modulated waveform as      %
%    noshift.m except it is doppler shifted with a change     %
%    consistent to the radar source moving at Mach 1.         %
%                                                             %
%%%%%%%%%%%%%%%%%%%%%%%%%%%%%%%%%%%%%%%%%%%%%%%%%%%%%%%%%%%%%%%%%


samples = 100;                          %Number of samples per period

shiftn = 1.000002213;
%Frequency shift ammount according to a doppler shift of Mach 1

two = 1/samples*[1:2*samples];          %2 periods worth of values
four = 1/samples*[1:4*samples];         %4 periods worth of values

wavecd = amp * sin(2*shiftn*pi*four);   %the carrier waveform
wave1d = amp * sin(2*shiftn*pi*two+(pi/2));
                                        %the first modulated waveform
wave2d = amp * sin(2*shiftn*pi*two+(2*pi/7));
                                        %the second modulated waveform
waved = [wavecd wave1d wave2d wavecd];  %the wave form put togther


wavepowd = waved.^2;
%the power of the combined waveform

detectd = 0;
nwaved = [];
nwavepowd = [];

nwavepowavetotd = [];
for i = 1:realizations
    nwavepowsortd = [];
    nwavepowaved = [];
%     nwave = [nwave;noise(i,:)+wave];
    nwavepowd = [nwavepowd;(noise(i,:)+waved).^2];
    for j = 1:periods
        nwavepowaved = [nwavepowaved, mean(nwavepowd(i,(samples*(j-
1)+1):j*samples)) * ones(1,samples)];
    end
    nwavepowavetotd = [nwavepowavetotd; nwavepowaved];
    if(max(nwavepowavetotd(i,:)) > threshold)
      detectd = detectd + 1;
    end
%     nwavepowsort = sort(nwavepow(i,:));

end

%figure
%plot(nwavepow(i,:))
%hold on
%plot(threshold*ones(1,1200))
%plot(nwavepowavetot(i,:),'k')
%hold off

%detect
```

Matchdoppex.m: Creates ROC curves for matched filter

```
%clear

%wave = wavetotals(13,:);

realizations = 100;
samples = 10;                           %Number of samples per period

amp = 1e-1;                                 %amplitude of the waveform

two = 1/samples*[1:2*samples];          %2 periods worth of values
four = 1/samples*[1:4*samples];         %4 periods worth of values

wavec = sin(2*pi*four);                 %the carrier waveform
wave1 = sin(2*pi*two+(pi/2));           %the first modulated waveform
wave2 = sin(2*pi*two+(2*pi/7));         %the second modulated waveform
%wave = [wavec wave1 wave2 wavec];       %the wave form put togther
normval = max(abs(xcorr(wave,wave)));

N=length(wave);
jay = sqrt(-1);
delta=(1267/2100)*pi/(10*N);

noise = [];
%noise realizations used for probabilities of false alarm and detection

for i = 1:realizations                  %sets the noise array
    noise = [noise;randn(1,length(wave))];
end

periods = length(wave)/samples;
%number of periods in the waveform


thresholdvals = [];
%The noise corelated with the signal used to set a threshold value

for i = 1:realizations
    thresholdvals = [thresholdvals, abs(xcorr(wave,noise(i,:)))];
end

thresholdvals = (thresholdvals);
thresholdvals = sort(thresholdvals);

threshold = thresholdvals(ceil(length(thresholdvals))-1);


amps =[.005 .01 .02 .03 .04 .05 .06 .07 .08 .09 .1 .2 .3 .4 .5 .6 .7 .8
.9 1];
%All the amplitudes to be tested

detecttotdopp = [];

for trials = 1:length(amps)
    detecttot = [];
for d = 1:21
    nwave = [];
    for i = 1:realizations
        amp = amps(trials);
        nwave = [nwave;((amp.*wave) + noise(i,:))];
```

```
        for j = 1:N
            awavee(i,j)=nwave(i,j)*exp(-jay*delta*(j-1)*(d-1));
        end
    end


    detect = 0;
    for i = 1:realizations
        detectval = [];
        detectval = (abs(xcorr(wave,awavee(i,:))));
        if(max(detectval) > threshold)
            detect = detect + 1;
        end
    end
    detecttot = [detecttot, detect];

end
    detecttotdopp = [detecttotdopp;detecttot];
end


x=[0:21-1]/(21-1);
sigtono = 10 * log10(amps.^2/2);
mesh(x,sigtono,(detecttotdopp./realizations))
view(-340,20);
axis([0 1 sigtono(1) sigtono(length(sigtono)) 0 1])
v = axis;

%figure
%plot(sigtono,detecttot(1:20)/(realizations))
%hold on
%plot(sigtono,detecttot(1:20)/(realizations),'o')
%hold off
%title('ROC Curves for Matched Filter')
%xlabel('Signal to Noise Ratio (dB)')
%ylabel('Probability of Detection')
%axis([10*log10(amps(1)^2/2) 10*log10(amps(length(amps))^2/2) 0 1]);
%v = axis;
```

Bibliography

1. Gross, F., D. Soileau, L. Kremer, "Investigation of Optimal Codes or Code Sets for Enhanced Radar Performance." Final Report Contract No. USZA22-97-K-0001, December 1997

2. IEEE Standard Letter Designations for Radar-Frequency Bands, IEEE Std 521-1984

3. Nathanson, F. E., *Radar Design Principles*, Mendham NJ: Sci Tech, 1999

4. Skolnik, M. *Introduction to Radar Systems*, Third Edition, New York: McGraw-Hill, 2001

References

5. Jain, R. The Art of Computer Systems Performance Analysis, New York: John Wiley & Sons, 1991

6. Welti, G. R., "Quantitative Codes for Pulsed Radar," *IRE Trans. Inform. Theory*, vol. IT-6, pp. 400-408, June 1960

7. Frank, R. L., "Polyphase Codes with Good Nonperiodic Correlation Properties," *IEEE trans. Inform. Theory*, vol. IT-9, pp. 43-45, January 1963

REPORT DOCUMENTATION PAGE		*Form Approved* *OMB No. 074-0188*

The public reporting burden for this collection of information is estimated to average 1 hour per response, including the time for reviewing instructions, searching existing data sources, gathering and maintaining the data needed, and completing and reviewing the collection of information. Send comments regarding this burden estimate or any other aspect of the collection of information, including suggestions for reducing this burden to Department of Defense, Washington Headquarters Services, Directorate for Information Operations and Reports (0704-0188), 1215 Jefferson Davis Highway, Suite 1204, Arlington, VA 22202-4302. Respondents should be aware that notwithstanding any other provision of law, no person shall be subject to an penalty for failing to comply with a collection of information if it does not display a currently valid OMB control number.
PLEASE DO NOT RETURN YOUR FORM TO THE ABOVE ADDRESS.

1. REPORT DATE *(DD-MM-YYYY)* 25-03-2003	2. REPORT TYPE **Master's Thesis**	3. DATES COVERED *(From – To)* Aug 2002 – Mar 2003

4. TITLE AND SUBTITLE	5a. CONTRACT NUMBER
INVESTIGATION OF DOPPLER EFFECTS ON THE DETECTION OF POLYPHASE CODED RADAR WAVEFORMS	5b. GRANT NUMBER
	5c. PROGRAM ELEMENT NUMBER

6. AUTHOR(S)	5d. PROJECT NUMBER If funded, enter ENR #
Bowman, Geoffrey, G., 2Lt, USAF	5e. TASK NUMBER
	5f. WORK UNIT NUMBER

7. PERFORMING ORGANIZATION NAMES(S) AND ADDRESS(S) Air Force Institute of Technology Graduate School of Engineering and Management (AFIT/EN) 2950 Hobson Way, Building 640 WPAFB OH 45433-7765	8. PERFORMING ORGANIZATION REPORT NUMBER AFIT/GCE/ENG/03-01

9. SPONSORING/MONITORING AGENCY NAME(S) AND ADDRESS(ES) AFMC/AFRL/SNZT Attn: Mr. John D. Garcher 2241 Avionics Circle DSN: 785-3631 ext: 4311 WPAFB OH 45433-7765 e-mail: John.Garcher@wpafb.af.mil	10. SPONSOR/MONITOR'S ACRONYM(S)
	11. SPONSOR/MONITOR'S REPORT NUMBER(S)

12. DISTRIBUTION/AVAILABILITY STATEMENT

APPROVED FOR PUBLIC RELEASE; DISTRIBUTION UNLIMITED.

13. SUPPLEMENTARY NOTES

14. ABSTRACT
Special operations missions often depend on discrete insertion of highly trained soldiers into dangerous territory. To reduce the risk involved in this type of engagement, Low Probability of Detection radar waveforms have been designed specifically to defeat enemy passive radar detectors. These waveforms have been shown to perform well when the Doppler shift is minimal, but their performance degrades dramatically with increased frequency shifts due to Doppler effects.

This research compares one known Low Probability of Detection waveform, based on Welti coding, with a radar waveform known to provide Doppler constancy, namely, one based on Frank coding. These waveforms are tested using a non-cooperative square-law passive detector as well as a cooperative matched filter detector for various Doppler shift values. Research conclusions address the question of whether or not the Frank coded waveforms provide better detection capability than Welti coded waveforms at high levels of Doppler shift.

Conclusions from this research indicate that there is no advantage to using Frank coded waveforms over Welti coded waveforms. All waveforms behaved the same at increasing Doppler shift levels for each of the detectors.

15. SUBJECT TERMS
   Radar, Doppler Radar, Radar Countermeasures, Radar Receivers, Radar Correlation, Radar Pulses
   Signals, Radar Interception, Defense Systems

16. SECURITY CLASSIFICATION OF:			17. LIMITATION OF ABSTRACT	18. NUMBER OF PAGES	19a. NAME OF RESPONSIBLE PERSON Steven C Gustafson, PhD (ENG)
a. REPORT	b. ABSTRACT	c. THIS PAGE			19b. TELEPHONE NUMBER *(Include area code)*
U	U	U	UU	87	(937) 255-3636, ext 4598; e-mail: Stephen.Gustafson@afit.edu

Standard Form 298 (Rev. 8-98)
Prescribed by ANSI Std. Z39-18